Article

Cell Reports

Regulation of Cellular Senescence by Polycomb Chromatin Modifiers through Distinct DNA Damage- and Histone Methylation-Dependent Pathways

Graphical Abstract

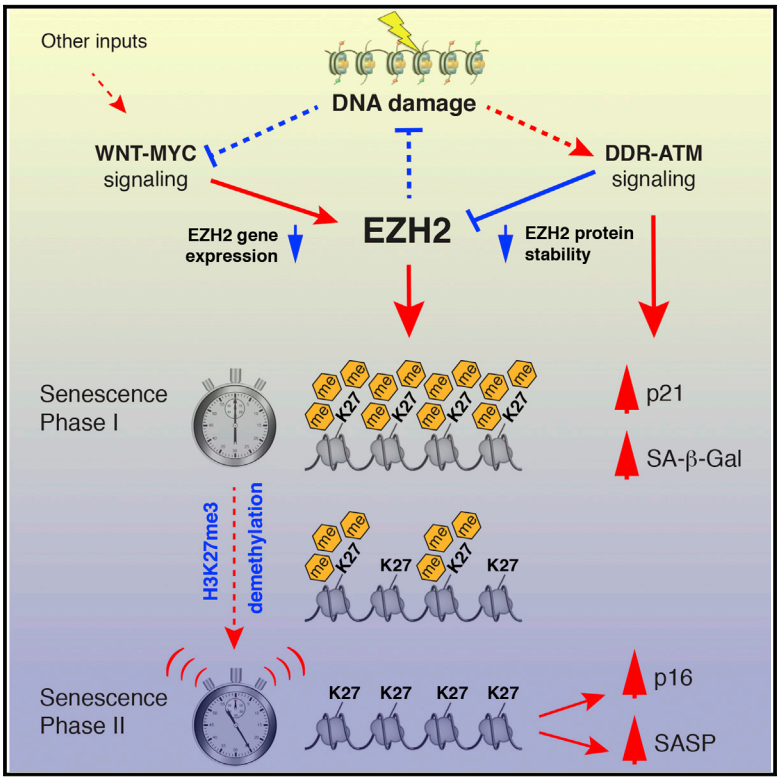

Authors

Takahiro Ito, Yee Voan Teo, Shane A. Evans, Nicola Neretti, John M. Sedivy

Correspondence

john_sedivy@brown.edu

In Brief

Ito et al. show that downregulation of EZH2 rapidly elicits DNA damage and triggers the onset of senescence without loss of H3K27me3 marks. With slower kinetics, the depletion of H2K27me3 results in the upregulation of p16 and proinflammatory factors. WNT-MYC and ATM signaling are identified as upstream regulators of EZH2.

Highlights

- Depletion of EZH2 elicits DNA damage in a replication-dependent manner
- EZH2 is regulated by the WNT-MYC pathway and DDR-mediated proteolysis
- Removal of H3K27me3 induces senescence in the absence of DNA damage
- H3K27me3 marks act as a timer that links DNA damage with the induction of SASP

Data and Software Availability

GSE109064

Ito et al., 2018, Cell Reports 22, 3480–3492
March 27, 2018 © 2018 The Author(s).
https://doi.org/10.1016/j.celrep.2018.03.002

CellPress

OPEN ACCESS
CellPress

Cell Reports
Article

Regulation of Cellular Senescence by Polycomb Chromatin Modifiers through Distinct DNA Damage- and Histone Methylation-Dependent Pathways

Takahiro Ito,[1,3] Yee Voan Teo,[1] Shane A. Evans,[2] Nicola Neretti,[1,2] and John M. Sedivy[1,4,*]
[1]Department of Molecular Biology, Cell Biology and Biochemistry, Brown University, Providence, RI 02912, USA
[2]Center for Computational Molecular Biology, Brown University, Providence, RI 02912, USA
[3]Present address: Broad Institute of MIT and Harvard, 415 Main Street, Cambridge, MA 02142, USA
[4]Lead Contact
*Correspondence: john_sedivy@brown.edu
https://doi.org/10.1016/j.celrep.2018.03.002

SUMMARY

Polycomb group (PcG) factors maintain facultative heterochromatin and mediate many important developmental and differentiation processes. EZH2, a PcG histone H3 lysine-27 methyltransferase, is repressed in senescent cells. We show here that downregulation of *EZH2* promotes senescence through two distinct mechanisms. First, depletion of *EZH2* in proliferating cells rapidly initiates a DNA damage response prior to a reduction in the levels of H3K27me3 marks. Second, the eventual loss of H3K27me3 induces p16 (*CDKN2A*) gene expression independent of DNA damage and potently activates genes of the senescence-associated secretory phenotype (SASP). The progressive depletion of H3K27me3 marks can be viewed as a molecular "timer" to provide a window during which cells can repair DNA damage. *EZH2* is regulated transcriptionally by WNT and MYC signaling and posttranslationally by DNA damage-triggered protein turnover. These mechanisms provide insights into the processes that generate senescent cells during aging.

INTRODUCTION

Cellular senescence is the irreversible loss of replicative capacity triggered by genotoxic stresses such as telomere erosion (Sulli et al., 2012). It is an important component of normal physiological processes such as development, wound healing, and aging (Campisi, 2013). Expression of activated oncogenes (such as the G12V variant of *HRAS*) in normal cells leads to what is known as oncogene-induced senescence (OIS) (Serrano et al., 1997). Senescent cells accumulate to low levels in normal tissues with age, and their clearance in mice delays age-associated phenotypes (Baker et al., 2016; Herbig et al., 2006).

Senescent cells show characteristic changes in gene expression, including upregulation and secretion of proinflammatory cytokines, chemokines, and extracellular matrix-remodeling enzymes, referred to as the senescence-associated secretory phenotype (SASP) (He and Sharpless, 2017). Formation of localized regions of heterochromatin known as senescence-associated heterochromatic foci (SAHF) can be observed in some cell types (Narita et al., 2003). The cell cycle arrest is mediated by upregulation of the cyclin-dependent kinase inhibitors p21 (*CDKN1A*) and p16 (*CDKN2A*). p21 is upregulated by the tumor suppressor p53 (*TP53*), an important sensor of stresses, including DNA damage. p16 is regulated in a more complex manner that includes the Polycomb group (PcG) of chromatin regulators (Gil and Peters, 2006).

The PcG proteins are epigenetic regulators that maintain gene expression patterns established during development or differentiation (epigenetic is defined as heritable effects without changes in DNA sequence). They are found in two families of complexes, known as Polycomb repressive complex 1 and 2 (PRC1 and PRC2). PRC2 contains EZH2, the histone lysine methyltransferase that catalyzes the trimethylation of lysine 27 on histone H3 (H3K27me3) through its conserved Su(var)3-9, Enhancer-of-zeste and Trithorax (SET) domain. PRC1 and PRC2 act in concert to promote an inactive chromatin environment that represses transcription. During senescence, some PcG proteins are downregulated, leading to loss of H3K27me3 at the *CDKN2A* locus, which results in the upregulation of p16 (Bracken et al., 2007). However, PcG proteins likely have additional roles beyond suppression of p16 during senescence (Shah et al., 2013).

Growing evidence suggests that EZH2 plays vital functions independent of its role to catalyze trimethylation of H3K27. EZH2 has been reported to act as a coactivator of the androgen receptor (Xu et al., 2012). EZH2 can also methylate non-histone substrates (Kim et al., 2013; Lee et al., 2012). Additionally, certain cancer cells appear to depend on both methyltransferase-dependent and -independent functions of EZH2 (Kim et al., 2015). However, it remains unclear whether loss of EZH2 affects senescence through catalytic or non-catalytic mechanisms.

Few studies have addressed the regulation of PcG during the onset of senescence. One possible upstream effector is wingless-type mouse mammary tumor virus integration site (WNT) signaling, whose downregulation has been found to induce senescence (Ye et al., 2007). In the canonical WNT pathway, extracellular WNT proteins ultimately upregulate a variety of target genes, including *MYC*. Further evidence for a possible regulatory link is that the *BMI1* gene, a PRC1 component, is a direct MYC target and that downregulation of MYC can promote senescence (Guney et al., 2006).

This is an open access article under the CC BY-NC-ND license (http://creativecommons.org/licenses/by-nc-nd/4.0/).

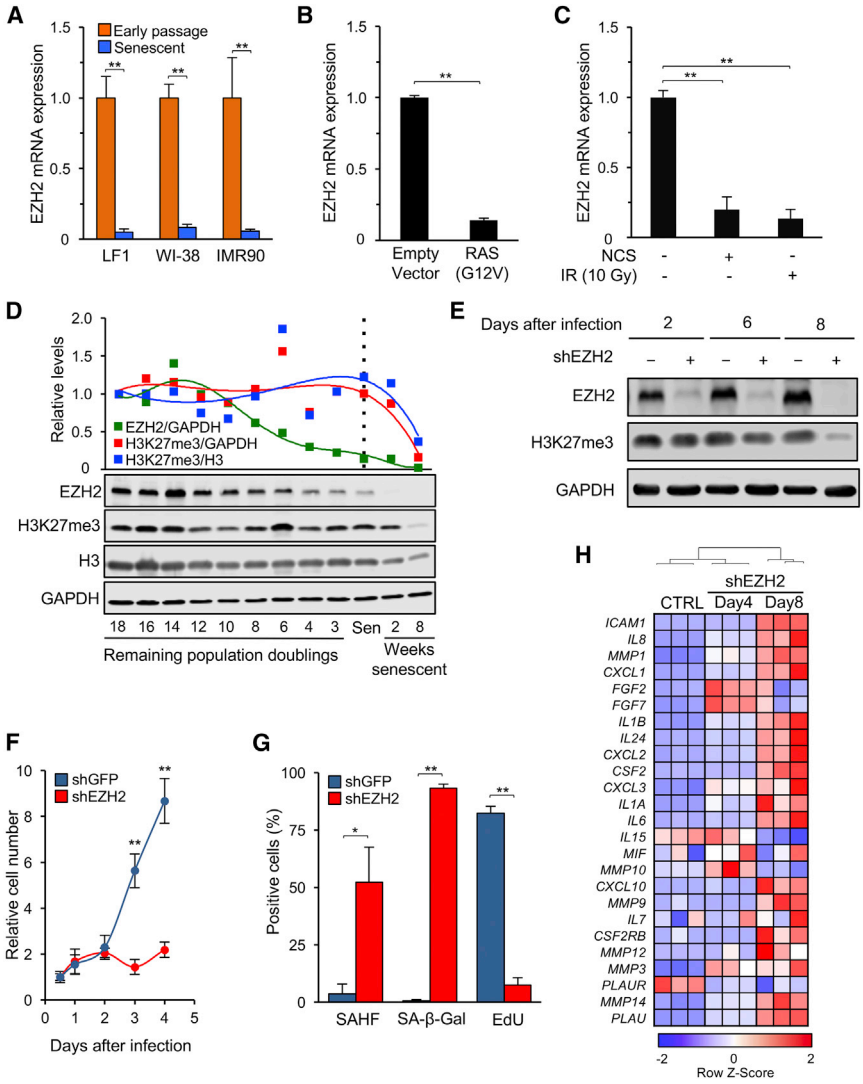

Figure 1. EZH2 Expression Decreases during Senescence, and Its Acute Downregulation Elicits Premature Senescence

(A) *EZH2* mRNA levels were determined by real-time qPCR in early-passage proliferating and replicatively senescent cells of strains LF1, WI-38, and IMR90 (**$p < 0.01$, $n = 3$).

(B) Early passage LF1 cells were infected with a lentivirus vector expressing *HRAS*(G12V) cDNA (or empty vector control), and expression of *EZH2* mRNA was determined 6 days after infection. (**$p < 0.01$, $n = 3$).

(C) Cells were irradiated with ionizing radiation (10 Gy) or treated with 200 ng/mL neocarzinostatin (NCS), and *EZH2* mRNA levels were determined after 6 days (**$p < 0.01$, $n = 3$).

(D) EZH2 protein levels and the presence of K27me3 marks on H3 were examined in LF1 cells by immunoblotting, from 18 population doublings before senescence until 8 weeks after the onset of senescence. EZH2 and H3K27me3 levels were normalized to GAPDH (green, red); H3K27me3 is also shown normalized to total H3 (blue).

(E) Cells were infected with a lentivirus vector expressing shRNA 3 against *EZH2* (Figure S1H). shRNA to GFP was the control. The levels of EZH2 and H3K27me3 were examined by immunoblotting.

(F) *EZH2* was knocked down as in (E), and proliferation was assessed by counting cell numbers (**$p < 0.01$, $n = 3$).

(G) The presence of SAHF, SA-β-Gal activity, and EdU incorporation were determined 2 days after shEZH2 infection. SA-β-Gal or SAHF-positive cells were scored as percent of total cells in randomly selected fields (*$p < 0.05$, **$p < 0.01$, $n = 3$).

(H) *EZH2* was knocked down as in (E), and unsupervised hierarchical clustering of SASP gene *Z* scores from RNA-seq data is shown as heatmaps. Error bars represent SD. See also Figures S1 and S2 and Tables S1, S4, and S5.

Here we report that downregulation of *EZH2* induces senescence by an H3K27me3-independent mechanism by activating a DNA damage response (DDR) during DNA replication. However, with delayed kinetics, loss of the H3K27me3 modification at the *CDKN2A* locus induces senescence by upregulating p16 in a DNA damage-independent manner. The loss of H3K27me3 also promotes the transcription of SASP genes. Upstream regulators of EZH2 include posttranslational modification by the ataxia telangiectasia mutated (ATM) kinase and transcriptional regulation by the WNT-MYC pathway.

RESULTS

Downregulation of *EZH2* Leads to Cellular Senescence with Features of SASP

Expression profiling of proliferating and replicatively senescent human diploid fibroblasts (HDFs) showed that *EZH2* is among the genes that are reproducibly downregulated in senescent cells (Lackner et al., 2014). Real-time qPCR) confirmed that *EZH2* transcripts were decreased in senescent cells of three commonly used strains of normal HDFs (LF1, WI-38, and IMR90) (Figure 1A). In addition, cells made senescent by expression of *HRAS*(G12V) or exposure to DNA-damaging agents also showed reduced expression of *EZH2* (Figures 1B and 1C). The levels of EZH2 protein decreased gradually as cells approached replicative senescence (Figures 1D and S1A). EZH2 protein became undetectable after 2 weeks of senescence; however, depletion of the H3K27me3 mark was not apparent until much later. Although we observed some loss of core histone H3 during senescence (Ivanov et al., 2013), this did not account for the reduction of H3K27me3 marks. Similar to LF1 cells, WI-38 and IMR90 cells showed loss of EZH2 at (or shortly after) the onset of senescence, whereas the disappearance of H3K37me3 lagged (Figure S1B). Although EZH2 levels are reduced in quiescence (~2-fold), senescent cells show an essentially complete depletion (Figures S1C and S2D). Synchronous induction of

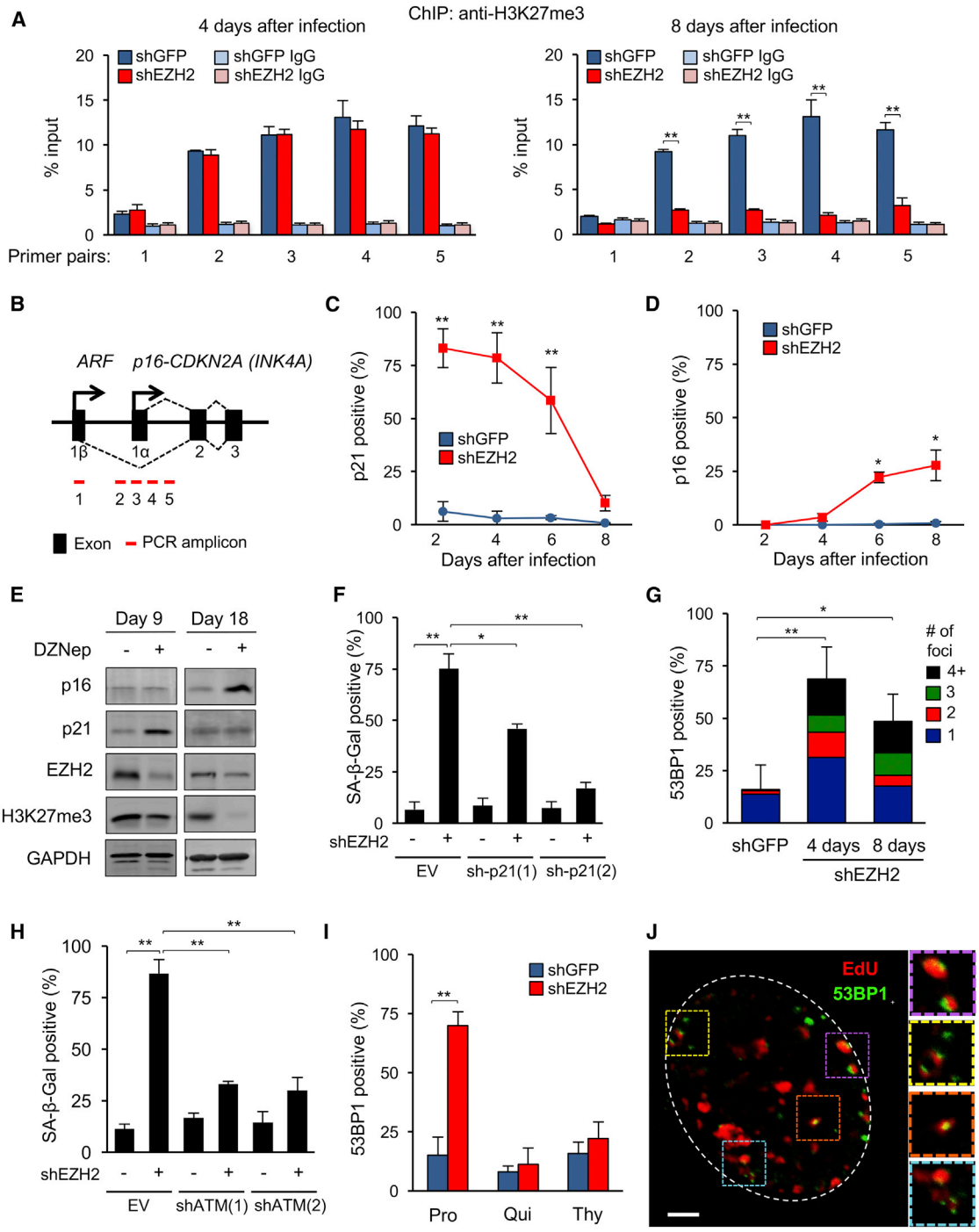

Figure 2. Downregulation of EZH2 Induces DNA Damage and Senescence in a DNA Replication-Dependent Manner

(A) H3K27me3 enrichment at the *CDKN2A* locus was determined 4 and 8 days after shEZH2 infection using ChIP. For locations of primer pairs, see (B). Normal rabbit immunoglobulin G (IgG) was used as the immunoprecipitation (IP) control (**$p < 0.01$, n = 3).

(B) Schematic of the *CDKN2A* locus.

(C) The frequency of p21-expressing cells was scored by IF after knockdown of *EZH2* (percent of total cells, random fields, more than 400 cells per condition, **$p < 0.01$).

(D) The frequency of p16-expressing cells was determined as in (C) (*$p < 0.05$).

(E) Early passage LF1 cells were grown in the presence of DZNep (5 μM), and the levels of p16, p21, and EZH2 proteins and H3K27me3 marks were examined by immunoblotting after 9 and 18 days of treatment.

(legend continued on next page)

senescence by DNA damage (etoposide) rapidly reduced EZH2 levels without accompanying changes in global H3K27me3 marks (Figures S1E and S1F).

To confirm that downregulation of *EZH2* is sufficient to induce senescence, we introduced short hairpin RNAs (shRNAs) targeting its transcript into early-passage LF1 cells (Figure S1G). Three distinct shRNAs were tested using lentivirus vectors and resulted in a 63%–97% decrease of *EZH2* mRNA (Figure S1H). Knockdown of *EZH2* resulted in rapid depletion of EZH2 protein 2 days after infection, whereas significant depletion of H3K27me3 was not evident until 8 days (Figure 1E). Downregulation of *EZH2* induced premature senescence by several criteria. First, cell proliferation was arrested within 2 days (Figure 1F). Second, the cells expressed senescence-associated β-galactosidase (SA-β-Gal), displayed SAHF, and did not incorporate 5-ethynyl-2′ deoxyuridine (EdU) (Figures 1G and S1I). In accordance with the presence of SAHF, the levels of the histone variant macroH2A increased (Figures S1J and S1K; Ye et al., 2007). Third, RNA sequencing (RNA-seq) analysis showed expression of SASP and inflammatory genes after *EZH2* knockdown (Figures 1H and S2A and S2B). Interestingly, this phenotype became prominent only at late times after infection (6–8 days), whereas growth arrest, SA-β-Gal, and SAHF were induced much more rapidly (2–4 days). Collectively, downregulation *EZH2* is sufficient to rapidly induce senescence accompanied by a robust SASP response.

Downregulation of *EZH2* Results in DNA Damage and Induces p21

Because global levels of H3K27me3 were not affected at the onset of replicative senescence or senescence induced by knockdown of *EZH2*, we examined the presence of H3K27me3 marks at the *CDKN2A* locus by performing chromatin immunoprecipitation (ChIP) coupled with qPCR (ChIP-qPCR). No significant changes in H3K27me3 enrichment were observed 4 days after infection with shEZH2, with a decrease becoming apparent at 8 days (Figures 2A and 2B). These data reflect closely the global levels of H3K27me3 and suggest that loss of *EZH2* can induce senescence independent of epigenetic changes at the *CDKN2A* locus.

Four days after knockdown of *EZH2*, RNA-seq analysis of differential gene expression implicated p53 and p21 activation as the top upstream regulators (Figure S2C). To examine the activation of senescence pathways elicited by the downregulation of *EZH2* in more detail, we monitored the time course of p21 and p16 expression changes. p21 mRNA was induced 4 days after *EZH2* knockdown (Figure S3A), whereas p16 mRNA was unchanged at this time, becoming upregulated only later (8 days; Figure S3B). The earliest time after infection we could assess was 2 days, at which point SA-β-Gal staining showed that the majority of cells (93%) were already senescent (Figure 1G). Likewise, examining single cells by immunofluorescence, we found that, at the 2-day time point, 83% of cells were positive for p21 protein (Figure 2C). The frequency of p21-positive cells declined over time, with only 10% of cells being positive at 8 days.

A similar analysis of p16 showed no expression at early time points, with the appearance of p16-positive cells becoming significant at 6 and 8 days (Figure 2D). In agreement, treatment with the drug 3-deazaneplanocin A (DZNep), which is known to deplete cellular EZH2 protein levels (Tan et al., 2007), induced senescence characterized by early activation of p21 followed by upregulation of SASP genes and p16 and loss of H3K27me3 marks (Figures 2E and S3C and S3D). To examine whether upregulation of p21 is required for the induction of senescence by *EZH2* depletion, we performed double knockdowns and found that p21 knockdown opposed the appearance of senescent cells (Figures 2F and S3E–S3G). Collectively, these results indicate that p21 is an important and early effector engaged by *EZH2* downregulation, and that p16 upregulation occurs later and coincides with the loss of H3K27me3 at the *CDKN2A* locus.

Because the primary regulator of p21 in senescence is p53, which, in turn, is activated by DNA damage, we examined components of the DDR after knockdown of *EZH2*. Knockdown of *EZH2* led to a strong and rapid induction of 53BP1 DNA damage foci. Quantification of individual cells showed a significant increase in the frequency of both focus-containing cells as well as the number of foci per nucleus (Figure 2G).

To determine whether activation of ATM is required for the induction of senescence by *EZH2* downregulation, we performed double knockdowns of ATM and EZH2. We found that ATM knockdown significantly alleviated the onset of senescence (Figures 2H and S3H and S3I). To determine whether the DDR elicited by *EZH2* downregulation is localized to telomeres, we performed an assay that colocalizes DNA damage foci with telomeres (Herbig et al., 2006). We did not find significant changes in DNA damage occurring specifically at telomeres upon knockdown of *EZH2* (Figures S3J and S3K). Similarly, knockdown of *EZH2* in LF1 cells immortalized by expression of telomerase robustly induced senescence, as indicated by SA-β-Gal staining (Figure S3L), suggesting that telomere maintenance is not sufficient to prevent senescence because of *EZH2* depletion. Altogether, these data indicate that senescence elicited by *EZH2* downregulation is triggered initially by non-telomeric double-strand breaks (DSBs) and mediated by the ATM-p53-p21 DDR pathway.

(F) p21 shRNAs or the empty vector were combined with an *EZH2* shRNA (+) or a shGFP control (−), and SA-β-Gal-positive cells were scored 4 days after infection (*$p < 0.05$, **$p < 0.01$, $n = 3$).
(G) 53BP1 foci were visualized by IF 4 and 8 days after *EZH2* knockdown. The stacked bars depict the fraction of cells with 1 focus (blue) or 2 (red), 3 (green), and more than 4 (black) foci per nucleus (**$p < 0.01$, $n = 4$).
(H) shATM and shEZH2 knockdowns were combined, and SA-β-Gal-positive cells were scored as in (F) (**$p < 0.01$, $n = 3$).
(I) At the time of shEZH2 infection (time [t] = 0; Figure S1G), cells were reseeded into either normal medium (Pro, 15% FBS), quiescence-inducing medium (Qui, 0.25% FBS), or medium supplemented with thymidine (Thy). 53BP1 foci were scored after 4 days (**$p < 0.01$, $n = 3$).
(J) *EZH2* was knocked down as in (A), and cells were pulse-labeled with EdU for 1 hr 2 days after infection. A representative image showing colocalization of EdU (red) and 53BP1 (green) signals is shown. Right: magnified views of the indicated areas. Scale bar, 3 μm.
Error bars represent SD. See also Figures S3 and S4 and Tables S1 and S2.

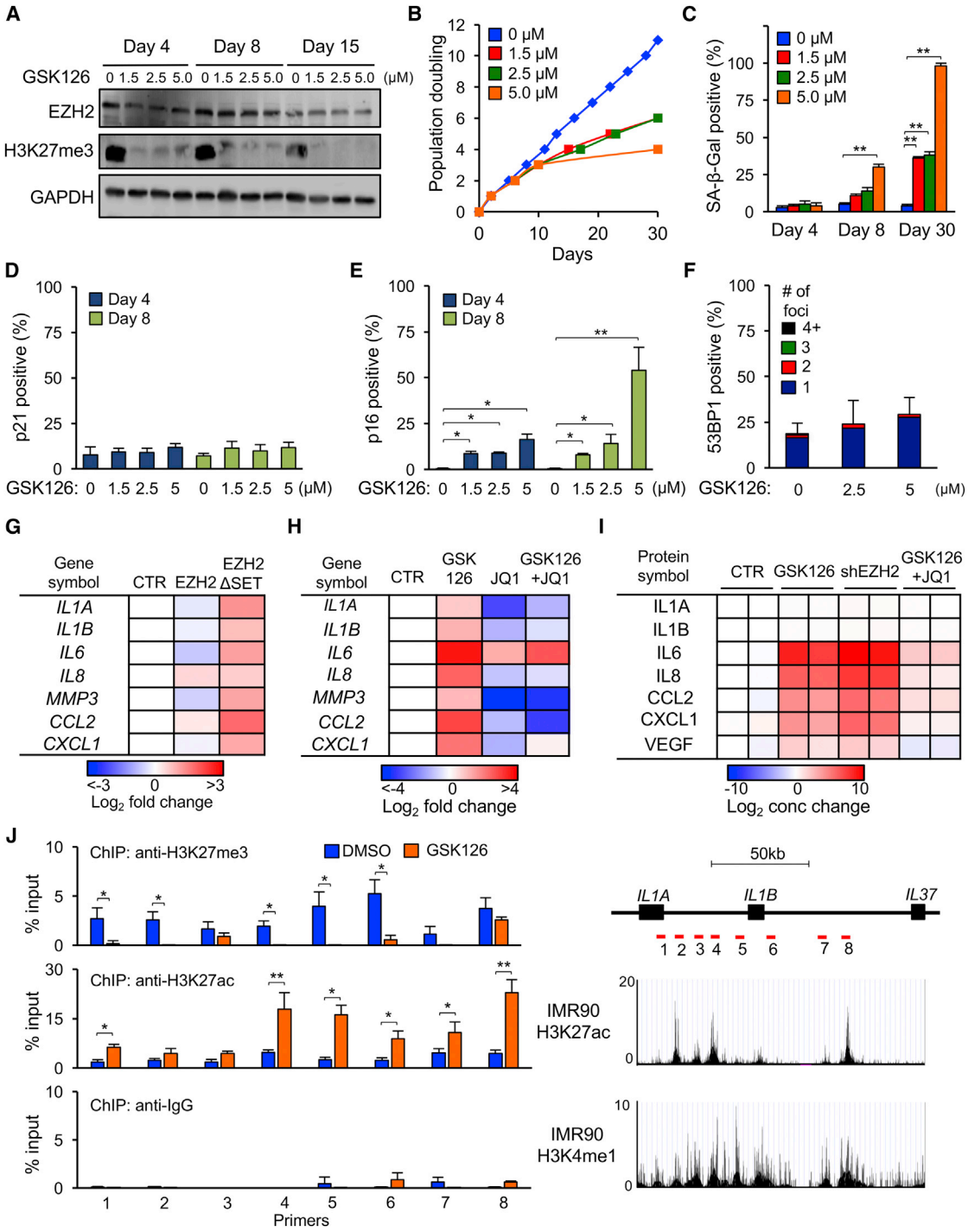

Figure 3. Inhibition of EZH2 Activity Induces Senescence in the Absence of DNA Damage by Depleting H3K27me3 Marks and Activating p16 and SASP Genes

(A) Early passage LF1 cells were grown continuously in the presence of GSK126, and levels of EZH2 protein and H3K27me3 marks were examined by immunoblotting.

(B and C) Cells were treated with GSK126 as in (A), and proliferation (B) or SA-β-Gal staining (C) were determined (**$p < 0.01$, $n = 3$).

(D and E) Cells were treated as in (A), and the frequency of p21-positive (D) and p16-positive (E) cells was scored by IF (percent of total cells, random fields, more than 400 cells per condition, *$p < 0.05$, **$p < 0.01$).

(F) Cells were treated with GSK126 for 8 days and examined for 53BP1 foci as in Figure 2G ($n = 3$).

(legend continued on next page)

Induction of DNA Damage by EZH2 Depletion Is Dependent on DNA Replication

Because EZH2 and other PRC2 components localize to sites of DNA replication (Hansen et al., 2008; Leung et al., 2013), and RNA-seq analysis showed the top downregulated ontologies upon knockdown of EZH2 to be associated with DNA strand elongation, DNA replication, and G1-S phase transition (Figure S2A), we examined the effect of cell cycle progression on the ability of *EZH2* knockdown to elicit a DDR. We found that arresting the cell cycle, either in G0 by serum withdrawal or in late G1 by a thymidine block, strongly protected against DDR induction, upregulation of p21, and onset of senescence (Figures 2I and S3M and S3N). To determine whether DNA damage localizes to sites of DNA replication, we knocked down *EZH2* under proliferative conditions and pulse-labeled with EdU before the cultures became fully senescent. We found that, in many of the cells still capable of EdU incorporation, 53BP1 foci frequently colocalized with sites of EdU labeling (Figure 2J). This is in agreement with recent studies showing that loss of PcG proteins affects the symmetry and progression of DNA replication forks and promotes their collapse (Piunti et al., 2014). Altogether, these data suggest that the DDR and ensuing senescence triggered by *EZH2* depletion are dependent on DNA replication.

To further examine the mechanism by which *EZH2* depletion induces replication fork stress, we ablated the recognition of the H3K27me3 mark by the PRC2 component EED. EED-H3K27me3 interaction was perturbed in two ways: with a small-molecule inhibitor (EED226) that blocks the H3K27me3-binding pocket of EED (Qi et al., 2017) and by expressing EED mutants unable to bind H3K27me3 marks (Margueron et al., 2009). Treatment with EED226 strongly induced the presence of SA-β-Gal-positive cells, upregulation of both p21 and p16, the appearance of 53BP1 DNA damage foci, and activation of a SASP response (Figures S4A–S4F). Similarly, ectopic expression of a mutant EED (F97A, W364A, or Y365A) unable to bind H3K27me3 elicited a DDR and upregulated SASP genes (Figures S4G and S4H), albeit to a lesser extent than treatment with EED226. In aggregate, these data suggest that the mislocalization or depletion of the PRC2 complex away from the replication fork induces a DDR through replication fork stress.

Loss of H3K27me3 Marks Induces Senescence by Upregulating p16 and SASP in a DNA Damage-Independent Manner

The temporal correlations between declining H3K27me3 levels, p16 upregulation, and activation of SASP genes suggest a possible contribution of H3K27me3 loss to the phenotypes of senescent cells. We therefore examined the effects of GSK126, a highly selective *S*-adenosyl-methionine (SAM)-competitive inhibitor of EZH2, on early-passage HDFs (McCabe et al., 2012). GSK126 inhibited EZH2 enzymatic activity within 4 days of treatment, as indicated by the loss of H3K27me3, without altering EZH2 protein levels (Figure 3A). Treatment with GSK126 also elicited senescence in a dose-dependent manner, as evidenced by the inhibition of proliferation and increase in SA-β-Gal staining. These effects were first evident at 8–10 days and continued to increase over a period of 30 days (Figures 3B and 3C and S5A).

To gain further insights into how loss of the H3K27me3 modification induces senescence, we investigated the expression of p21 and p16 proteins using single-cell immunofluorescence (IF) assays. Treatment of cells with GSK126 significantly increased the frequency of p16-positive cells but had no effect on p21 expression (Figures 3D and 3E). Furthermore, in contrast to knockdown of *EZH2*, inhibition of its activity with GSK126 did not elicit a DDR (Figure 3F), which agrees with the absence of p21 induction. To explore another method of inhibiting EZH2 activity, we used a catalytically inactive EZH2 mutant that lacks the conserved SET domain (EZH2ΔSET). Similar to what was observed after treatment with GSK126, infection with an EZH2ΔSET-expressing lentivirus vector induced senescence, accompanied by upregulation of p16 without triggering a DDR or upregulating p21 (Figures S5B–S5E).

To investigate the effects of EZH2 inhibition in non-replicating cells, quiescent LF1 cells were treated with GSK126 and monitored for changes in H3K27me3 and p16 levels. Although GSK126 treatment effectively depleted H3K27me3 marks within 4 days in proliferating cells (Figure 3A), it took at least 21 days to observe appreciable changes in quiescent cells (Figures S5F and S5G). Hence, loss of EZH2 methyltransferase activity can deplete H3K27me3 marks and induce p16 independent of cell cycle progression, albeit with much reduced kinetics.

H3K27me3 marks have been reported to decrease at enhancer regions of many SASP genes during senescence (Shah et al., 2013). In contrast, senescence leads to an increase in histone H3 lysine 27 acetyl (H3K27ac) at enhancers adjacent to SASP genes (Tasdemir et al., 2016). SASP factors were broadly upregulated and secreted following treatment with GSK126 or EZH2ΔSET-expressing lentivirus (Figures 3G–S3I). We therefore examined whether loss of H3K27me3 is associated with enrichment of H3K27ac at enhancers of SASP genes. Indeed, we found, using ChIP-qPCR, that treatment of proliferating cells with GSK126 resulted in a decrease of H3K27me3

(G) Cells were infected with lentivirus vectors expressing *EZH2* cDNA, *EZH2* with an in-frame deletion of the SET domain (*EZH2ΔSET*), or empty vector control, and expression of the indicated genes was determined by real-time qPCR 9 days after infection. Data are represented as heatmaps relative to control cells (n = 3).
(H) Cells were treated with GSK126 (5 μM), JQ1 (100 nM), or both, and expression of the indicated genes was determined by real-time qPCR after 10 days. Data are represented as heatmaps relative to DMSO-treated cells (n = 3).
(I) Cytokine array analysis of conditioned medium from cells treated with GSK126 (5 μM) or GSK126 plus JQ1 (100 nM) for 17 days. For comparison, cells were infected with shRNAs against *EZH2* (shEZH2) or GFP (control [CTR]) for 8 days. IL1A and IL1B were secreted at undetectable levels, as reported previously (Orjalo et al., 2009), because they remain cell surface-associated. Data are represented as heatmaps relative to CTR (n = 2). See Table S3 for the measured cytokine concentrations.
(J) Cells were treated with GSK126 (5 μM) or DMSO for 10 days, and H3K27me3 and H3K27ac enrichment at the *IL1A-IL1B-IL37* loci was determined by ChIP-qPCR. Primer pairs were chosen in regions of putative enhancers, and their locations are shown in the schematic as red bars. H3K27ac and H3K4me1 tracks were obtained from ENCODE (GEO: GSM469966 and GSM521895). Normal rabbit IgG was used as the IP control (*$p < 0.05$, **$p < 0.01$, n = 3).
Error bars represent SD. See also Figure S5 and Tables S1, S2, and S3.

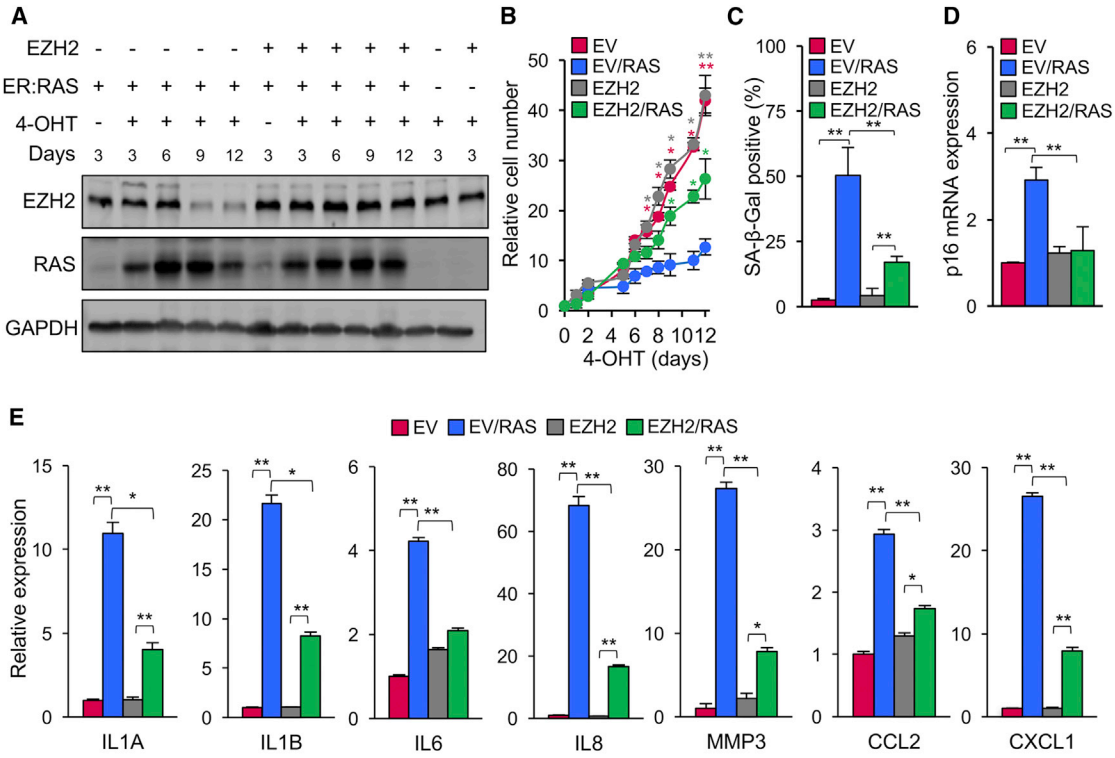

Figure 4. Expression of EZH2 Opposes Entry into OIS and Induction of SASP

(A) LF1 cells were engineered using lentivirus vectors to stably express *EZH2* cDNA and a 4-OHT-inducible ER:RAS(G12V) protein. Control cell lines were constructed using empty vectors. Cells were treated with 4-OHT (200 nM) or vehicle (ethanol) for the indicated times, and the levels of EZH2 and ER:RAS proteins were determined by immunoblotting.

(B) Proliferation in the experiment shown in (A) was assessed by counting cell numbers (*$p < 0.05$, **$p < 0.01$, $n = 3$).

(C) SA-β-Gal-positive cells were scored after 12 days of 4-OHT treatment in the experiment shown in (A) (**$p < 0.01$, $n = 3$).

(D) p16 mRNA expression was determined by real-time qPCR as in (C) (**$p < 0.01$, $n = 3$).

(E) Expression of the indicated SASP genes was determined by real-time qPCR as in (C) (*$p < 0.05$, **$p < 0.01$, $n = 3$).

Error bars represent SD. See also Table S1.

and increase of H3K27ac marks at annotated enhancers adjacent to *IL1A* and *IL1B* (Figure 3J) and *MMP3* (Figure S5H) genes.

Members of the bromodomain and extraterminal domain (BET) family of proteins are the "readers" that recognize acetylated lysine residues and facilitate transcriptional activation by recruitment of co-regulatory complexes. Accordingly, treatment with the small molecule BET inhibitor JQ1 antagonized the expression and secretion of GSK126-induced SASP factors (Figures 3H and 3I). However, JQ1 did not affect the GSK126-elicited upregulation of p16 or rescue senescence (Figures S5I and S5J). These data suggest that the H3K27 methylation-to-acetylation switch at enhancers of SASP genes mediates their activation but does not have broader effects on senescence.

SASP gene expression in senescent cells is also regulated, in part, by the mammalian target of rapamycin (mTOR) (Laberge et al., 2015). mTOR activity promotes the translation of the cytokine IL1A, which is then processed at the membrane and binds the IL1R receptor, which, in turn, activates the degradation of IκB, an inhibitor of nuclear factor κB (NF-κB) transcription factors. We found that, in GSK126-treated cells, the mTOR inhibitor rapamycin reduced the transcript levels of some SASP genes upregulated by GSK126 (Figure S5K). Treatment with GSK126 also decreased the levels of IκBα (Figure S5L), and this was rescued by treatment with rapamycin, Hence, NF-κB and mTOR contribute to the regulation of SASP genes during GSK126-induced senescence in a manner that is shared with other forms of senescence. In aggregate, these experiments indicate that inhibition of EZH2 methyltransferase activity is sufficient to induce senescence in the absence of DNA damage and that this response is characterized by the upregulation of p16 and accompanied by SASP.

EZH2 Suppresses Entry into Oncogene-Induced Senescence

We next examined whether preventing the downregulation of *EZH2* that normally occurs during senescence could antagonize its establishment. We induced OIS using a 4-hydroxytamoxifen (4-OHT)-inducible estrogen receptor (ER):RAS(G12V) fusion protein and combined this with ectopic expression of *EZH2* cDNA delivered with a lentivirus vector (Figure 4A). Expression of *EZH2* strongly alleviated entry into OIS, as indicated by cell proliferation, frequency of SA-β-Gal positive cells, and p16 expression (Figures 4B–4D). Additionally, EZH2 also broadly alleviated

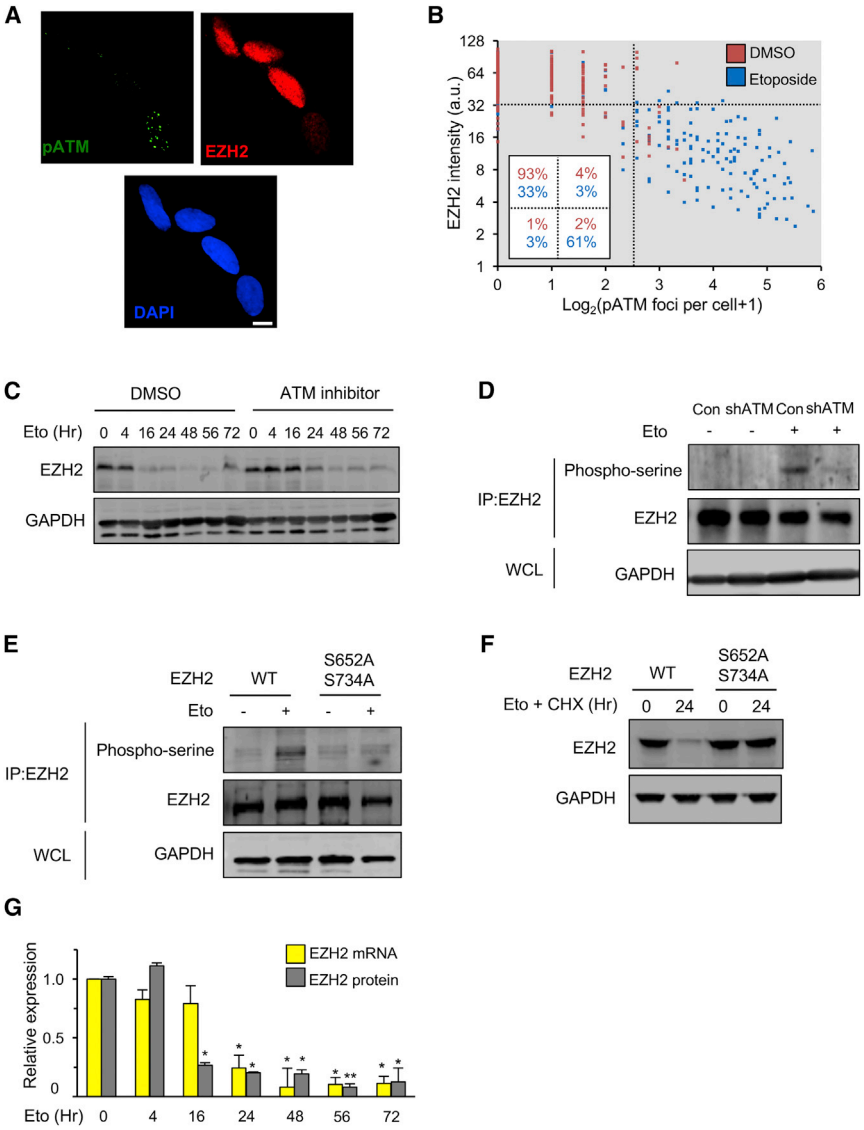

Figure 5. DNA Damage-Mediated Degradation of EZH2

(A) LF1 cells were treated with etoposide (40 μM) for 8 hr and immunostained with antibodies to phospho-ATM (S1981, green) or EZH2 (red). Nuclei were counterstained with DAPI (blue). The same image is shown in the three channels. Scale bar, 10 μm.

(B) Cells were treated with etoposide for 20 hr, stained as in (A), and scored for EZH2 intensity and the number of phospho-ATM (S1981) foci per nucleus (random fields, more than 200 cells per condition).

(C) Cells were treated with etoposide (Eto) plus the ATM inhibitor KU-55933 (10 μM) or carrier (DMSO), and the levels of EZH2 protein were determined by immunoblotting.

(D) Cells infected with lentivirus vectors expressing shRNA against *ATM* (or empty vector as control) were treated for 8 hr with etoposide (+) or DMSO vehicle (−). Cell lysates were immunoprecipitated with anti-EZH2 antibody, followed by immunoblotting analysis with anti-phospho-serine or anti-EZH2 antibodies. Aliquots of whole cell lysates (WCLs) were immunoblotted for GAPDH to verify equivalent total protein input.

(E) Cells engineered using lentivirus vectors to stably express *EZH2* or *EZH2*(S652A/S734A) mutant cDNAs were processed and analyzed as in (D).

(F) *EZH2* or *EZH2*(S652A/S734A) mutant cDNA-expressing cells were treated with etoposide and cycloheximide (CHX, 50 μg/mL), and the levels of EZH2 protein were determined by immunoblotting.

(G) Cells were treated with etoposide in a time course, and the relative levels of *EZH2* mRNA and EZH2 protein were determined by real-time qPCR and immunoblotting, respectively. The p values shown are pairwise comparisons with the zero time point (*$p < 0.05$, **$p < 0.01$, $n = 3$).

Error bars represent SD. See also Figure S6 and Table S1.

the induction of SASP genes (Figure 4E). These data indicate that maintenance of *EZH2* expression and, hence, H3K27me3 marks suppresses entry into senescence in response to stress.

Regulation of *EZH2* Expression in Cellular Senescence

ATM kinase-mediated phosphorylation of EZH2 has been reported to decrease its stability (Li et al., 2013). In genotoxic stress-induced senescence, we found that cells with high numbers of phosphorylated ATM foci contained low levels of EZH2 (Figures 5A and 5B). In a time course experiment, the ATM inhibitor KU-55933 significantly delayed the disappearance of EZH2 protein (Figures 5C and S6A), and the MG132 proteasome inhibitor delayed the loss of EZH2 (Figure S6B). The phosphorylation of EZH2 on serine residues elicited by etoposide was inhibited by shRNA knockdown of ATM (Figure 5D). EZH2 is phosphorylated by ATM at Ser652 and Ser734 during neurodegeneration (Li et al., 2013). EZH2 serine phosphorylation and turnover in response to etoposide were both alleviated in cells ectopically expressing an S652A/S743A double mutant of *EZH2* (Figures 5E and 5F). Collectively, these data indicate that EZH2 protein, in a process initiated by ATM, is rapidly degraded during the DDR at the onset of senescence.

Interestingly, *EZH2* mRNA expression was also downregulated during the onset of senescence, but with slower kinetics than that of EZH2 protein (Figure 5G). This suggests that DNA damage also affects *EZH2* expression transcriptionally. Expression of the WNT ligand WNT2 has been reported to decrease in both replicative senescence and OIS (Ye et al., 2007), and MYC is a well-known downstream effector of WNT signaling (Herbst et al., 2014). We found that WNT2 and MYC are both downregulated, that the activity of β-catenin declines in cells undergoing replicative senescence (Figure 6A and S6C), and that

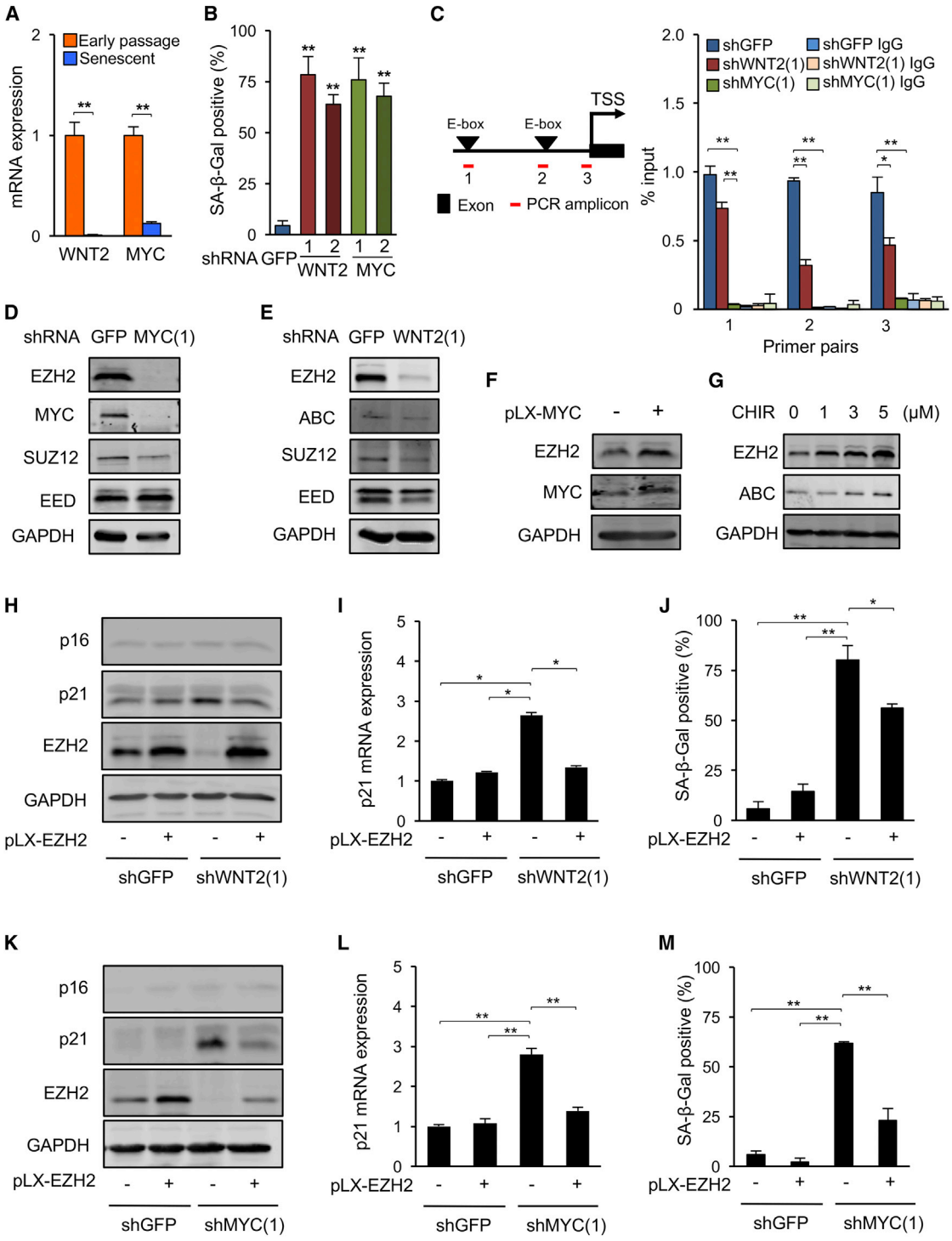

Figure 6. EZH2 Is Required for Senescence Induced by Downregulation of WNT or MYC Signaling

(A) *WNT2* and *MYC* mRNA levels were determined by real-time qPCR in early-passage proliferating and replicatively senescent (2 weeks, Figure 1D) LF1 fibroblasts (**$p < 0.01$, n = 3).

(B) LF1 cells were infected with lentivirus vectors expressing shRNAs against *WNT2* or *MYC*, and SA-β-Gal-positive cells were scored 4 days after infection. shGFP was used as the control (**$p < 0.01$, n = 3).

(C) MYC enrichment at the promoter region of the *EZH2* gene was determined by ChIP after knockdown of *WNT2* or *MYC* as in (B). Locations of primer pairs are shown on the left. Normal rabbit IgG was used as the IP control (*$p < 0.05$, **$p < 0.01$, n = 3).

(D) Cells were infected with shRNA (#1) targeting *MYC* as in (B), and the levels of MYC, EZH2, SUZ12, and EED proteins were determined by immunoblotting.

(legend continued on next page)

knockdown of either WNT2 or MYC is sufficient to induce senescence and proliferation arrest (Figures 6B and S6D–S6F).

MYC is a direct regulator of *BMI1*, a PRC1 component (Guney et al., 2006). We thus examined whether WNT and MYC signaling also regulate *EZH2* during senescence. Examination of Encyclopdia of DNA elements (ENCODE) datasets revealed a broad region of MYC binding centered at 150 bp upstream of the transcriptional start site (TSS) of the *EZH2* gene. We therefore performed quantitative ChIP analysis with several primer pairs and found that MYC is indeed recruited to this region in proliferating cells (Figure 6C). Binding was reduced in cells after knockdown of WNT2 and eliminated after knockdown of MYC. These results show that EZH2 is a direct transcriptional target of MYC.

Knockdown of MYC strongly downregulated *EZH2*, with weaker effects observed on other PRC2 proteins (Figure 6D). Similar results were found after knockdown of WNT2 (Figure 6E). Conversely, ectopic expression of *MYC* cDNA increased EZH2 protein levels (Figure 6F). Finally, activation of WNT signaling with the GSK-3 inhibitor CHIR99021 increased the levels of both active β-catenin and EZH2 proteins in a concentration-dependent manner (Figure 6G). These data indicate that WNT signaling and MYC act upstream of *EZH2* to regulate its expression.

To test whether EZH2 is a necessary component of this pathway, we knocked down WNT2 or MYC in cells that were previously engineered to ectopically express *EZH2* cDNA. Ectopic expression of *EZH2* suppressed the activation of p21 and partially rescued the onset of senescence after WNT2 knockdown (Figures 6H–6J and S6G). Similarly, expression of *EZH2* alleviated the activation of p21 and onset of senescence after knockdown of MYC (Figures 6K–6M and S6G). This analysis thus places EZH2 downstream of both WNT2 and MYC. To confirm that MYC is acting downstream of WNT2, we knocked down WNT2 in cells ectopically expressing *MYC* cDNA and found that activation of p21 and entry into senescence were alleviated (Figures S6H–S6J). These data further confirm the existence of a WNT-MYC-EZH2 pathway for the regulation of senescence.

DISCUSSION

In this study, we have explored how PcG regulates cellular senescence. The EZH2 protein is the catalytic core of PcG complexes, depositing the H3K27me3 mark that is the characteristic feature of facultative heterochromatin. We found that downregulation of *EZH2* with shRNA in normal, proliferating cells rapidly induced senescence that was initiated by widespread DNA damage, leading to a DDR mediated by the ATM-p53-p21 pathway. The ensuing cell cycle arrest clearly preceded the depletion of H3K27me3 marks and is therefore likely to be independent of expression changes at PcG-regulated loci. PcG complexes are known to be localized at replication forks during S phase (Hansen et al., 2008; Piunti et al., 2014), and their depletion can cause DNA damage through replication fork collapse. The DDR caused by loss of *EZH2* likely proceeds through this mechanism because it was dependent on cell cycle progression, and DNA damage (53BP1) foci frequently colocalized with sites of DNA replication. Additionally, prevention of PRC2 localization to the replication fork by antagonizing the binding of EED to H3K27me3 marks phenocopied the effect of EZH2 depletion. Replication fork collapse because of over-replication elicited by oncogenes such as H-RAS has been implicated as the triggering mechanism of OIS (Di Micco et al., 2006).

The CDK inhibitor p16 (CDKN2A) is an important effector of senescence and was rapidly upregulated upon EZH2 knockdown. However, the upregulation of p16 was a late event after EZH2 depletion, clearly separated from the appearance of DNA damage, induction of SA-β-Gal activity, and cell cycle arrest. The induction of senescence by PcG downregulation thus consists of two distinct phases: an early phase characterized by DNA damage and a late phase caused by depletion of H3K27me3 marks. That these processes can be independent was evidenced by the activation of senescence by the simple inhibition of EZH2 activity, either with the drug GSK126 or expression of a catalytically inactive EZH2 protein. These senescence responses were late in onset and characterized by the upregulation of p16 but devoid of DNA damage and activation of p21.

Although irreversible cell cycle arrest is the classical feature of senescence, senescent cells display many gene expression changes that are involved in unrelated processes. Among these, the SASP is of considerable interest because it is likely to be responsible for many of the deleterious effects of senescent cells. p16 is an important regulator of senescence, but its upregulation alone, although sufficient to cause cell cycle arrest,

(E) Cells were infected with shRNA (#1) against *WNT2* as in (B), and the levels of active β-catenin (ABC), EZH2, SUZ12, and EED proteins were examined by immunoblotting.
(F) Cells were infected with a lentivirus vector expressing *MYC* cDNA, and the levels of EZH2 and MYC proteins were determined by immunoblotting. Empty pLX vector (–) was used as the control.
(G) Cells were treated for 8 days with the indicated concentrations of the GSK3 inhibitor CHIR99021, and the levels of EZH2 and ABC proteins were determined by immunoblotting.
(H) Ectopic expression of *EZH2* cDNA was combined with a shRNA knockdown of *WNT2*. Controls were empty pLX vector for *EZH2* (–) and shGFP for *WNT2*. The levels of p16, p21, and EZH2 proteins were determined by immunoblotting. Note that, although endogenous EZH2 expression is effectively downregulated by shWNT2 (lane 3; see also E), ectopic expression is maintained by the pLX-EZH2 vector (lane 4).
(I) p21 mRNA expression was determined by real-time qPCR in the experiment shown in (H) (*$p < 0.05$, $n = 3$).
(J) The frequency of SA-β-Gal-positive cells was scored in the experiment shown in (H) (*$p < 0.05$, **$p < 0.01$, $n = 3$).
(K) The double intervention shown in (H) was performed with *MYC* shRNA (instead of *WNT2* shRNA), and the levels of p16, p21, and EZH2 proteins were examined. Note again that, although endogenous *EZH2* expression is effectively downregulated by shMYC (lane 3; see also D), ectopic expression is maintained by the pLX-EZH2 vector (lane 4).
(L) p21 mRNA expression was determined in the experiment shown in (K) (**$p < 0.01$, $n = 3$).
(M) SA-β-Gal-positive cells were quantified in the experiment shown in (K).
Error bars represent SD. See also Figure S6 and Tables S1 and S2.

does not induce the SASP (Coppé et al., 2011). We found that GSK126-mediated loss of H3K27me3 marks resulted not only in the upregulation of p16 but also a robust activation of SASP genes. This was associated with a replacement of H3K27me3 by H3K27ac at enhancers of SASP genes, whose activation was opposed by BET inhibitors, suggesting that these epigenetic changes have functional significance. The observation that loss of EZH2 activity can upregulate SASP genes in the absence of a DDR underscores the importance of PcG-mediated epigenetic regulation.

How is EZH2 regulated during senescence? At the transcriptional level, we document here the existence of a WNT2-MYC-EZH2 regulatory cascade. Downregulation of MYC closely phenocopied the senescence response induced by depletion of *EZH2*, including DNA damage, biphasic kinetics, and activation of SASP. We also found that *EZH2* is a direct transcriptional target of MYC. MYC has been reported to downregulate miR-26a/b, a negative effector of EZH2 (Sander et al., 2008), and, through its effects on the AKT pathway, to indirectly activate and stabilize the EZH2 protein (Kaur and Cole, 2013). These mechanisms likely reinforce the direct regulation of the *EZH2* gene by MYC we document here and underscore the importance of MYC as a regulator of EZH2 and, by extension, the PcG pathway.

Because canonical WNT signaling is known to activate MYC expression, we examined the regulatory relationships between WNT2, MYC, and EZH2 during the onset of senescence, a situation of reduced WNT and MYC signaling. We did this by an epistasis analysis, performing a series of double interventions. In particular, ectopic expression of MYC antagonized the senescence-inducing effects of WNT2 depletion, and, likewise, expression of *EZH2* partially reversed the effects of both MYC and WNT2 downregulation. These compensatory effects were significant but not complete, most likely because other PcG genes in addition to EZH2 are involved, and overexpression of MYC in normal cells can trigger either apoptosis or senescence. Nevertheless, the genetic relationships are clearly indicative of a WNT2-MYC-EZH2 hierarchy.

EZH2 is also regulated posttranslationally by ATM-triggered protein degradation (Li et al., 2013). We found that genotoxic stress-induced senescence was accompanied by the rapid disappearance of EZH2 protein that was faster than its transcriptional repression and was antagonized by the ATM inhibitor KU-55933 and the proteasome inhibitor MG132. EZH2 is rapidly recruited to sites of DNA damage after laser micro-irradiation (Chou et al., 2010). These findings suggest that PcG plays a role in the response to DNA damage and is then processed for degradation. We propose that the rapid disappearance of both *EZH2* mRNA and protein we have documented at the onset of cellular senescence can act as a "clock" that determines the length of the first, DDR-associated phase of senescence. The slow, DNA replication-independent turnover of H3K27me3 marks would be the timing mechanism, whose depletion eventually triggers the upregulation of p16 and SASP genes and, thus, ushers in the second (probably irreversible) phase of senescence. In agreement, ectopic expression of *EZH2* significantly delayed the upregulation of p16 as well as many SASP genes.

The SASP is activated by DNA damage through an ATM-mediated DDR (Rodier et al., 2009). IL1A is an important SASP regulator (Laberge et al., 2015) that, in concert with mTOR, activates the NF-κB transcription factors. Our data indicate that EZH2 is an important factor in the initial upregulation of the *IL1A* gene. First, GSK126 was an effective inducer of SASP in the absence of a DDR, thus effectively placing EZH2 between the DNA damage signal and *IL1A* upregulation. Second, mTOR and NF-κB influenced SASP gene expression in GSK126-induced senescence, again placing EZH2 in an upstream position. Finally ectopic expression of *EZH2* delayed SASP during OIS. NF-κB activity is also promoted by GATA4 during senescence (Kang et al., 2015), and GATA4 has been reported to be repressed by EZH2 methylation (He et al., 2012). This mechanism, which acts upstream of the IL1A-mTOR-NF-κB pathway, would thus also be enforced by loss of EZH2 activity.

Our model, as shown in the Graphical Abstract, places DNA damage both upstream and downstream of EZH2. Following acute DNA damage, such as telomere uncapping or irradiation, the ATM-mediated DDR is likely sufficient to upregulate p21 and initiate the first phase of senescence. However, during OIS, which is ultimately caused by replication fork collapse, the DNA damage elicited by the depletion of EZH2 at these sites may be an important reinforcing mechanism. Furthermore, during senescence mediated by the WNT-MYC pathway in the absence of upstream DNA damage, DNA damage because of EZH2 downregulation provides the signal to establish cell cycle arrest and, hence, is an important component of the "timer" that provides an opportunity for repair.

Our results suggest that inhibiting components of PcG complexes is likely to induce senescence phenotypes through a variety of mechanisms. Understanding these will be critical for teasing out the anti-cancer effects of PcG inhibitors from possible deleterious consequences. For example, compromise of facultative heterochromatin maintenance might lead to upregulation of the SASP and proinflammatory effects in normal resting cells. Given that PcG complexes are localized at replication forks for the transmission of H3K27me3 marks to daughter cells, targeting this process may be an effective way to provoke DNA damage that is largely confined to cycling cells.

EXPERIMENTAL PROCEDURES

Culture Conditions

All HDF cultures were passaged (1:4) and incubated at 37°C in an atmosphere of 2.5% O_2, 92.5% N_2, and 5% CO_2. 293T cells were cultured in air supplemented with 5% CO_2. LF1 cells were cultured in Ham's F10 nutrient mixture (Invitrogen) supplemented with 15% fetal bovine serum (FBS, HyClone). Quiescence was induced by reducing FBS to 0.25%. IMR90, WI-38, and 293T cells were cultured in DMEM supplemented with 10% FBS. All media were supplemented with 2 mM L-glutamine and penicillin/streptomycin (Sigma-Aldrich).

Lentiviral Infections

293T cells were co-transfected with plasmid DNAs of a lentiviral vector and the helper vectors pVSV-G and pCMV Δ8.9 using FuGENE HD (Promega). Medium was collected 24, 36, and 48 hr after transfection and used to infect HDF cells. Infected cells were selected with 2 μg/mL puromycin for 2 days, 500 μg/mL G418 for 3 days, or 5 μg/mL blasticidin for 5 days (see Figure S1G for a schematic of the time line and Supplemental Experimental Procedures for details of individual vectors).

Real-Time qPCR

Real-time qPCR was performed using the SYBR Green system (Applied Biosystems) on the ABI 7900 Fast Sequence Detection instrument as specified by the manufacturer. Total RNA was harvested from cells using Trizol reagent (Invitrogen) and further purified using RNeasy columns (QIAGEN). 1 μg of total RNA was transcribed into cDNA in 50-μL reactions using the TaqMan kit (Applied Biosystems). 1 μL of this reaction was used in subsequent real-time qPCR reactions. GAPDH was used as the normalization control. All reactions were performed in triplicates. The primers used for real-time qPCR are provided in Table S1.

ChIP

The procedure was based on the Magna ChIP protocol (Millipore, 17-10085) and Chromatrap Premium ChIP qPCR (Chromatrap, 500115). Cells (2×10^6) were cross-linked in 1% formaldehyde for 10 min at room temperature, harvested by scraping, centrifuged, and resuspended in SDS lysis buffer. After 10 min on ice, lysed cells were diluted 2-fold in ChIP dilution buffer and disrupted with the S220 Focused Ultrasonicator (Covaris) to yield genomic DNA fragments of 300 bp. The samples were immunoprecipitated overnight at 4°C with the indicated antibodies. Immunocomplexes were pulled down with 20 μL of magnetic protein A beads as described in the Magna ChIP protocol. The DNA was recovered by 2 hr digestion with proteinase K at 65°C, followed by a 10-min incubation at 95°C. The DNA was cleaned up by phenol/chloroform extraction and ethanol precipitation and finally resuspended in 30 μL of Tris-EDTA (TE).

The ChIP and input were then used for qPCR with the primers described in Table S2.

Immunofluorescence and Immuno-FISH

Cells were fixed for 20 min with freshly prepared 4% paraformaldehyde in PBS. Permeabilization was performed with 0.2% Triton X-100 in PBS for 20 min at room temperature. After blocking nonspecific binding, antibodies were diluted in the blocking solution and incubated with the specimens overnight at 4°C in a humidified chamber. Samples were washed three times with PBS and incubated for 1 hr at room temperature with secondary antibodies diluted in blocking solution. Nuclei were counterstained with 2 μg/mL DAPI in PBS containing 0.2% Triton X-100 for 15 min. The telomere dysfunction-induced focus (TIF) assay, an immunofluorescence combined with fluorescence in situ hybridization (Immuno-FISH) procedure (Herbig et al., 2006) is described in detail in the Supplemental Experimental Procedures, as is a listing of the antibodies used. For EdU pulse labeling, cells were incubated with 10 μM of EdU stock solution (Click-iT, Invitrogen) for 1 hr prior to fixation.

Statistical Analysis

Data are shown as means with SD. Statistical significance was determined using the two-tailed Student's test (t test). $p < 0.05$ was considered significant.

DATA AND SOFTWARE AVAILABILITY

The accession number for the RNA-seq data reported in this paper is GEO: GSE109064.

SUPPLEMENTAL INFORMATION

Supplemental Information includes Supplemental Experimental Procedures, six figures, and five tables and can be found with this article online at https://doi.org/10.1016/j.celrep.2018.03.002.

ACKNOWLEDGMENTS

This work was supported by NIH/NIA grants R37 AG016694 and P01 AG051449 (to J.M.S.). T.I. was supported in part by NIH grants T32 GM007601 and F31 AG043189. The Brown Genomics Core was supported in part by the COBRE award from NIH/NIGMS P30 GM0103410.

AUTHOR CONTRIBUTIONS

Conceptualization and Methodology, T.I. and J.M.S.; Investigation, T.I., S.A.E., and Y.V.T.; Writing – Original Draft and Review and Editing, T.I. and J.M.S.; Supervision, N.N. and J.M.S.

DECLARATION OF INTERESTS

The authors declare no competing interests.

Received: July 10, 2017
Revised: January 9, 2018
Accepted: February 28, 2018
Published: March 27, 2018

REFERENCES

Baker, D.J., Childs, B.G., Durik, M., Wijers, M.E., Sieben, C.J., Zhong, J., Saltness, R.A., Jeganathan, K.B., Verzosa, G.C., Pezeshki, A., et al. (2016). Naturally occurring p16(Ink4a)-positive cells shorten healthy lifespan. Nature *530*, 184–189.

Bracken, A.P., Kleine-Kohlbrecher, D., Dietrich, N., Pasini, D., Gargiulo, G., Beekman, C., Theilgaard-Mönch, K., Minucci, S., Porse, B.T., Marine, J.C., et al. (2007). The Polycomb group proteins bind throughout the INK4A-ARF locus and are disassociated in senescent cells. Genes Dev. *21*, 525–530.

Campisi, J. (2013). Aging, cellular senescence, and cancer. Annu. Rev. Physiol. *75*, 685–705.

Chou, D.M., Adamson, B., Dephoure, N.E., Tan, X., Nottke, A.C., Hurov, K.E., Gygi, S.P., Colaiácovo, M.P., and Elledge, S.J. (2010). A chromatin localization screen reveals poly (ADP ribose)-regulated recruitment of the repressive polycomb and NuRD complexes to sites of DNA damage. Proc. Natl. Acad. Sci. USA *107*, 18475–18480.

Coppé, J.P., Rodier, F., Patil, C.K., Freund, A., Desprez, P.Y., and Campisi, J. (2011). Tumor suppressor and aging biomarker p16(INK4a) induces cellular senescence without the associated inflammatory secretory phenotype. J. Biol. Chem. *286*, 36396–36403.

Di Micco, R., Fumagalli, M., Cicalese, A., Piccinin, S., Gasparini, P., Luise, C., Schurra, C., Garre', M., Nuciforo, P.G., Bensimon, A., et al. (2006). Oncogene-induced senescence is a DNA damage response triggered by DNA hyper-replication. Nature *444*, 638–642.

Gil, J., and Peters, G. (2006). Regulation of the INK4b-ARF-INK4a tumour suppressor locus: all for one or one for all. Nat. Rev. Mol. Cell Biol. *7*, 667–677.

Guney, I., Wu, S., and Sedivy, J.M. (2006). Reduced c-Myc signaling triggers telomere-independent senescence by regulating Bmi-1 and p16(INK4a). Proc. Natl. Acad. Sci. USA *103*, 3645–3650.

Hansen, K.H., Bracken, A.P., Pasini, D., Dietrich, N., Gehani, S.S., Monrad, A., Rappsilber, J., Lerdrup, M., and Helin, K. (2008). A model for transmission of the H3K27me3 epigenetic mark. Nat. Cell Biol. *10*, 1291–1300.

He, S., and Sharpless, N.E. (2017). Senescence in Health and Disease. Cell *169*, 1000–1011.

He, A., Shen, X., Ma, Q., Cao, J., von Gise, A., Zhou, P., Wang, G., Marquez, V.E., Orkin, S.H., and Pu, W.T. (2012). PRC2 directly methylates GATA4 and represses its transcriptional activity. Genes Dev. *26*, 37–42.

Herbig, U., Ferreira, M., Condel, L., Carey, D., and Sedivy, J.M. (2006). Cellular senescence in aging primates. Science *311*, 1257.

Herbst, A., Jurinovic, V., Krebs, S., Thieme, S.E., Blum, H., Göke, B., and Kolligs, F.T. (2014). Comprehensive analysis of β-catenin target genes in colorectal carcinoma cell lines with deregulated Wnt/β-catenin signaling. BMC Genomics *15*, 74.

Ivanov, A., Pawlikowski, J., Manoharan, I., van Tuyn, J., Nelson, D.M., Rai, T.S., Shah, P.P., Hewitt, G., Korolchuk, V.I., Passos, J.F., et al. (2013). Lysosome-mediated processing of chromatin in senescence. J. Cell Biol. *202*, 129–143.

Kang, C., Xu, Q., Martin, T.D., Li, M.Z., Demaria, M., Aron, L., Lu, T., Yankner, B.A., Campisi, J., and Elledge, S.J. (2015). The DNA damage response induces inflammation and senescence by inhibiting autophagy of GATA4. Science *349*, aaa5612.

Kaur, M., and Cole, M.D. (2013). MYC acts via the PTEN tumor suppressor to elicit autoregulation and genome-wide gene repression by activation of the Ezh2 methyltransferase. Cancer Res. *73*, 695–705.

Kim, E., Kim, M., Woo, D.H., Shin, Y., Shin, J., Chang, N., Oh, Y.T., Kim, H., Rheey, J., Nakano, I., et al. (2013). Phosphorylation of EZH2 activates STAT3 signaling via STAT3 methylation and promotes tumorigenicity of glioblastoma stem-like cells. Cancer Cell *23*, 839–852.

Kim, K.H., Kim, W., Howard, T.P., Vazquez, F., Tsherniak, A., Wu, J.N., Wang, W., Haswell, J.R., Walensky, L.D., Hahn, W.C., et al. (2015). SWI/SNF-mutant cancers depend on catalytic and non-catalytic activity of EZH2. Nat. Med. *21*, 1491–1496.

Laberge, R.M., Sun, Y., Orjalo, A.V., Patil, C.K., Freund, A., Zhou, L., Curran, S.C., Davalos, A.R., Wilson-Edell, K.A., Liu, S., et al. (2015). MTOR regulates the pro-tumorigenic senescence-associated secretory phenotype by promoting IL1A translation. Nat. Cell Biol. *17*, 1049–1061.

Lackner, D.H., Hayashi, M.T., Cesare, A.J., and Karlseder, J. (2014). A genomics approach identifies senescence-specific gene expression regulation. Aging Cell *13*, 946–950.

Lee, J.M., Lee, J.S., Kim, H., Kim, K., Park, H., Kim, J.Y., Lee, S.H., Kim, I.S., Kim, J., Lee, M., et al. (2012). EZH2 generates a methyl degron that is recognized by the DCAF1/DDB1/CUL4 E3 ubiquitin ligase complex. Mol. Cell *48*, 572–586.

Leung, K.H., Abou El Hassan, M., and Bremner, R. (2013). A rapid and efficient method to purify proteins at replication forks under native conditions. Biotechniques *55*, 204–206.

Li, J., Hart, R.P., Mallimo, E.M., Swerdel, M.R., Kusnecov, A.W., and Herrup, K. (2013). EZH2-mediated H3K27 trimethylation mediates neurodegeneration in ataxia-telangiectasia. Nat. Neurosci. *16*, 1745–1753.

Margueron, R., Justin, N., Ohno, K., Sharpe, M.L., Son, J., Drury, W.J., 3rd, Voigt, P., Martin, S.R., Taylor, W.R., De Marco, V., et al. (2009). Role of the polycomb protein EED in the propagation of repressive histone marks. Nature *461*, 762–767.

McCabe, M.T., Ott, H.M., Ganji, G., Korenchuk, S., Thompson, C., Van Aller, G.S., Liu, Y., Graves, A.P., Della Pietra, A., 3rd, Diaz, E., et al. (2012). EZH2 inhibition as a therapeutic strategy for lymphoma with EZH2-activating mutations. Nature *492*, 108–112.

Narita, M., Nũnez, S., Heard, E., Narita, M., Lin, A.W., Hearn, S.A., Spector, D.L., Hannon, G.J., and Lowe, S.W. (2003). Rb-mediated heterochromatin formation and silencing of E2F target genes during cellular senescence. Cell *113*, 703–716.

Orjalo, A.V., Bhaumik, D., Gengler, B.K., Scott, G.K., and Campisi, J. (2009). Cell surface-bound IL-1alpha is an upstream regulator of the senescence-associated IL-6/IL-8 cytokine network. Proc. Natl. Acad. Sci. USA *106*, 17031–17036.

Piunti, A., Rossi, A., Cerutti, A., Albert, M., Jammula, S., Scelfo, A., Cedrone, L., Fragola, G., Olsson, L., Koseki, H., et al. (2014). Polycomb proteins control proliferation and transformation independently of cell cycle checkpoints by regulating DNA replication. Nat. Commun. *5*, 3649.

Qi, W., Zhao, K., Gu, J., Huang, Y., Wang, Y., Zhang, H., Zhang, M., Zhang, J., Yu, Z., Li, L., et al. (2017). An allosteric PRC2 inhibitor targeting the H3K27me3 binding pocket of EED. Nat. Chem. Biol. *13*, 381–388.

Rodier, F., Coppé, J.P., Patil, C.K., Hoeijmakers, W.A., Muñoz, D.P., Raza, S.R., Freund, A., Campeau, E., Davalos, A.R., and Campisi, J. (2009). Persistent DNA damage signalling triggers senescence-associated inflammatory cytokine secretion. Nat. Cell Biol. *11*, 973–979.

Sander, S., Bullinger, L., Klapproth, K., Fiedler, K., Kestler, H.A., Barth, T.F., Möller, P., Stilgenbauer, S., Pollack, J.R., and Wirth, T. (2008). MYC stimulates EZH2 expression by repression of its negative regulator miR-26a. Blood *112*, 4202–4212.

Serrano, M., Lin, A.W., McCurrach, M.E., Beach, D., and Lowe, S.W. (1997). Oncogenic ras provokes premature cell senescence associated with accumulation of p53 and p16INK4a. Cell *88*, 593–602.

Shah, P.P., Donahue, G., Otte, G.L., Capell, B.C., Nelson, D.M., Cao, K., Aggarwala, V., Cruickshanks, H.A., Rai, T.S., McBryan, T., et al. (2013). Lamin B1 depletion in senescent cells triggers large-scale changes in gene expression and the chromatin landscape. Genes Dev. *27*, 1787–1799.

Sulli, G., Di Micco, R., and d'Adda di Fagagna, F. (2012). Crosstalk between chromatin state and DNA damage response in cellular senescence and cancer. Nat. Rev. Cancer *12*, 709–720.

Tan, J., Yang, X., Zhuang, L., Jiang, X., Chen, W., Lee, P.L., Karuturi, R.K., Tan, P.B., Liu, E.T., and Yu, Q. (2007). Pharmacologic disruption of Polycomb-repressive complex 2-mediated gene repression selectively induces apoptosis in cancer cells. Genes Dev. *21*, 1050–1063.

Tasdemir, N., Banito, A., Roe, J.S., Alonso-Curbelo, D., Camiolo, M., Tschaharganeh, D.F., Huang, C.H., Aksoy, O., Bolden, J.E., Chen, C.C., et al. (2016). BRD4 Connects Enhancer Remodeling to Senescence Immune Surveillance. Cancer Discov. *6*, 612–629.

Xu, K., Wu, Z.J., Groner, A.C., He, H.H., Cai, C., Lis, R.T., Wu, X., Stack, E.C., Loda, M., Liu, T., et al. (2012). EZH2 oncogenic activity in castration-resistant prostate cancer cells is Polycomb-independent. Science *338*, 1465–1469.

Ye, X., Zerlanko, B., Kennedy, A., Banumathy, G., Zhang, R., and Adams, P.D. (2007). Downregulation of Wnt signaling is a trigger for formation of facultative heterochromatin and onset of cell senescence in primary human cells. Mol. Cell *27*, 183–196.

Cell Reports, Volume *22*

Supplemental Information

Regulation of Cellular Senescence by Polycomb Chromatin Modifiers through Distinct DNA Damage- and Histone Methylation-Dependent Pathways

Takahiro Ito, Yee Voan Teo, Shane A. Evans, Nicola Neretti, and John M. Sedivy

SUPPLEMENTAL INFORMATION

SUPPLEMENTAL EXPERIMENTAL PROCEDURES

Lentivirus Vector Procedures

Supernatants collected from 293T cells were filtered through a 0.45 μM filter. Infections of HDF cells were done in the presence of 8 μg/ml polybrene (Stewart et al., 2003). pLKO.1 vectors were used for shRNA-mediated gene knockdowns (Moffat et al., 2006). The control used throughout this study was an shRNA against an irrelevant target (GFP, 5'-TACAACAGCCACAACGTCTAT). The following shRNA vectors were obtained from Open Biosystems: EZH2, TRCN0000018365 (#1 in Figure S1H), TRCN0000040075 (#2 in Figure S1H), TRCN0000040076 (#3 in Figure S1H); WNT2, TRCN0000033373 (#1 in Figure S6D), TRCN0000033372 (#2 in Figure S6D), MYC, TRCN0000010390 (#1 in Figure S6E), TRCN0000039642 (#2 in Figure S6E); and CDKN1A (p21), TRCN0000287021 (#1 in Figure 2F), TRCN0000287091 (#2 in Figure 2F). A pSUPER retrovirus vector was used for the knockdown of ATM (5'-GATACCAGATCCTTGGAGA, #1 in Figure 2H) (Ortega-Atienza et al., 2015) and lentivirus vector for knockdown of ATM was a gift from Didier Trono (Addgene plasmid #14542, shATM#2 in Figure 2H). TRCN0000040076 (EZH2 #3) was used throughout this study. TRCN0000033373 and TRCN0000033372 (WNT2) corresponds to shWnt2-5 and shWnt2-4, respectively, described and validated by (Ye et al., 2007). TRCN0000010390 (MYC) was described and validated by (Guney et al., 2006). For double knockdowns of p21 and EZH2, and ATM and EZH2, early passage LF1 cells were infected with p21 or ATM shRNA vectors, drug selected, grown up as pools, and superinfected with EZH2 shRNA vectors. Full-length *EZH2* cDNA was obtained from the ATCC; *MYC* cDNA was a kind gift of Dr. Michael Cole (Dartmouth Medical School); *EED* was obtained from Applied Biological Materials. *EZH2* and *MYC* were PCR cloned into pLX303 (plasmid 25897, Addgene) modified by removal of the Gateway Destination sequences and incorporation of multiple cloning sites and sequence verified. *EZH2* and *EED* were also PCR cloned into pLenti-puro, gift from le-Ming Shih (Addgene plasmid #39481). Empty pLX and pLenti-puro vectors were used as controls. For the expression of *HRAS*(G12V) we used the lentivirus vector pLenti CMV RasV12 Neo (plasmid 22259, Addgene, in Figure 1B) or retrovirus vector pQCXIN CMV ER:RasV12 (kind gift of Dr. Gregory David, New York University School of Medicine, in Figure 4A-4E). ER:RasV12 was activated by continuous treatment with 200 ng/ml of 4-hydroxytamoxifen. The empty vector (plasmid 17485, Addgene) was used as the control. In combined cDNA expression and knockdown experiments, cells were first infected with *EZH2* or *MYC* cDNAs, stable pools were selected as indicated above, and subsequently infected with shRNA vectors.

Immunoblotting

Cells were harvested in Laemmli sample buffer (60 mM Tris pH 6.8, 2% SDS, 10% glycerol, 100 mM DTT). Whole cell extracts were separated by SDS-PAGE and transferred onto immobilon-FL membranes (Millipore). Signals were detected using the LI-COR Odyssey infrared imaging system (LI-COR Biosciences). Immunoblots shown are representative images of three independent experiments.

Antibodies Used

The antibodies used were as follows: Millipore, active β-catenin (05-665, 1:1000), H3K27me3 (07-449, 1:1000), EED (09-774, 1:2000), MYC (06-340, 1:2000), phosphoserine (05-1000,

1:1000); Cell Signaling, GAPDH (5174, 1:1000), histone H3 (4499, 1:1000), EZH2 (5246, 1:1000), SUZ12 (3737, 1:1000), IκBα (4814, 1:1000); Santa Cruz, p16 (sc-756, 1:500), p21 (sc-397, 1:200), lamin A/C (sc-6215, 1:200); BD Bioscience, RAS (610001, 1:1000).

Chromatin Immunoprecipitation

After crosslinking, formaldehyde was quenched by adding glycine to 125 mM, and the dishes were washed three times in ice-cold phosphate-buffered saline (PBS) containing 1x protease inhibitor (Roche). Composition of the SDS lysis buffer was 1% SDS, 10 mM EDTA, 50 mM Tris pH 8.1, 1x protease inhibitor cocktail. Composition of the ChIP dilution buffer was 0.01% SDS, 1.1% Triton X-100, 1.2 mM EDTA, 16.7 mM Tris-HCl pH 8.1, 167 mM NaCl. After sonication the samples were centrifuged and the supernatants were diluted five-fold with ChIP dilution buffer. An aliquot (1%) of each chromatin preparation was saved as input. Samples were immunoprecipitated with 4 μg of antibody to MYC (Millipore 06-340) or H3K27me3 (Millipore 07-449). After pulldown the magnetic protein A beads were washed once with each of low salt, high salt and LiCl wash buffers, followed by two washes with TE buffer. Final yields of DNA were quantified with the Qubit 2.0 dsDNA HS assay kit (Invitrogen, Q32851). For the Chromatrap Premium ChIP qPCR protocol, the IP slurry containing 1 μg of the sheared chromatin and 2 μg of antibody to H3K27me3 (as above) or H3K27ac (Cell Signaling, 8173S) were diluted in wash buffer 1, transferred into the Chromatrap spin column, and incubated for 6 hrs. at 4° on a rocking platform. The Chromatrap spin columns were washed with wash buffers and the DNA was eluted with 50 μl of elution buffer.

Immunoprecipitations

Cells were lysed in cell lysis buffer (20 mM Tris-HCl, 150 mM NaCl, 1 mM EDTA, 1 mM EGTA, 1% Triton, 2.5 mM sodium pyrophosphate, 1 mM beta-glycerophosphate, 1 mM Na_3VO_4, 1 μg/ml leupeptin, 1 mM PMSF) for 30 min. on ice and then passed through a 26.5-gauge needle three times. Cell lysates were incubated with anti-EZH2 antibody (Cell Signaling, 5246, 1:300) or control IgG overnight at 4°C. Pre-washed magnetic beads (Thermo Fisher Scientific, 11203D) were added to each sample and incubated for 6 hrs. at 4 °C. The beads were washed five times with cell lysis buffer, boiled at 100°C for 5 min. in Laemmli sample buffer and processed for immunoblotting.

RNA-seq

Cells were infected with a lentivirus vector expressing shRNA #3 against *EZH2* (Figure 1E-H) and cells were harvested at 4 and 8 days after infection. Total RNA was harvested from cells using Trizol reagent (Invitrogen) and further purified using the Purelink RNA Mini kit (Invitrogen) with DNase I digestion. RNA library preparation with polyA selection and Illumina HiSeq 2x150bp sequencing was performed by GeneWiz Inc. Paired-end reads were quality trimmed using Trim galore v0.4.0 and subsequently aligned to the human reference genome, hg19, using HISAT2 v2.1.0. Reads mapping to annotated genes were quantified using featureCounts (Liao et al., 2014). Differential gene expression was determined using DESeq2 v1.12.4 (Love et al., 2014) and significance was defined as FDR-corrected p-values of <0.05. The log2 fold change for each gene was used to rank the list of genes for GSEAPreranked analysis (Subramanian et al., 2005). FPKM values were calculated using DESeq2 and Z-scores were generated from FPKMs. Upstream regulators were identified using Ingenuity Pathway Analysis (IPA, Qiagen) with default settings. The cutoffs used were p <0.05 and absolute

fold-change >1.75. The differential expression and alignment rates are shown in Table S4, and the DESeq2 output for the entire dataset in Table S5.

Immunofluorescence and ImmunoFISH

Nonspecific binding solution contained 4% bovine serum albumin (BSA; Thermo Fisher Scientific), 2% donkey serum, and 0.1% Triton X-100 in PBS. The antibodies used were as follows: Santa Cruz, p16 (sc-756, 1:100), p21 (sc-397; 1:100); Millipore, γH2AX (05-636, 1:100); Becton Dickinson, 53BP1 (NB100-304, 1:100); Cell Signaling, phospho-ATM (Ser1981, 4526, 1:100), EZH2 (5246, 1:100). The rabbit polyclonal antibody against human mH2A was a kind gift from Dr. Peter Adams (University of Glasgow) and was used as indicated before (Kreiling et al., 2011). For the TIF assay (Herbig et al., 2004), cells were first fixed, permeabilized and immuno-stained for 53BP1 as described above. The samples were then dehydrated in a 70%, 90%, and 100% ethanol (3 min. each) and air dried. Nuclear DNA was denatured for 5 min. at 80°C in hybridization buffer containing 0.5 µg/ml Cy5-conjugated peptide nucleic acid (PNA) telomere C probe (PNA bio, #F1003), 70% formamide, 12 mM Tris HCl (pH 8), 5 mM KCl, 1 mM $MgCl_2$, 0.001% Triton X-100, and 2.5 mg/ml acetylated BSA. After denaturation, incubation was continued for 14 hrs. at room temperature in a humidified chamber. Cells were washed two times for 15 min. with 70% formamide in 2x SSC (0.3 M NaCl, 30 mM Na-citrate), followed by a 10 min. wash with 2x SSC, and a 10 min. wash with PBS. For EdU incorporation, cells were treated for 24 hours with EdU and processed as instructed by the manufacturer (Life Technologies, #C10337).

Cytokine Array

Cultures were washed three times with PBS and incubated in serum-free medium for 24 hrs. The conditioned media (CM) were collected and centrifuged at 1000 x g for 10 min. at 4°C. The CM were diluted in proportion to the cell number and analyzed using the Quantibody Human Cytokine Array 1 (QAH-CYT-1, RayBiotech) as per manufacturer's instructions. The signals were detected with a GenePix 4200B microarray scanner.

Detection of SA-β-Gal Activity

Cells grown on coverslips were fixed with 0.2% glutaraldehyde and 2% formaldehyde for 5 min., washed twice with PBS, and incubated overnight at 37°C in a staining solution (Debacq-Chainiaux et al., 2009) containing 5-bromo-4-chloro-3-indolyl-β-galactopyranoside.

Microscopy

Imaging was done on either a Zeiss Axiovert 200M fluorescence microscope equipped with a Roper CoolSnap HQ monochrome camera controlled by MetaMorph software 6.1 (Molecular Devices), or a Zeiss LSM 710 Confocal Laser Scanning Microscope. Image analysis was performed using ImageJ open source software from the NIH (http://rsbweb.nih.gov/ij/).

Site-directed mutagenesis

EZH2 mutant (S652A and S734A), EZH2 deletion (EZH2 Δ SET) and EED mutant (F97A, W364A, and Y365A) were generated by using the QuikChange Lightning Site-Directed Mutagenesis kit (Agilent Technologies). All constructs were confirmed by sequencing.

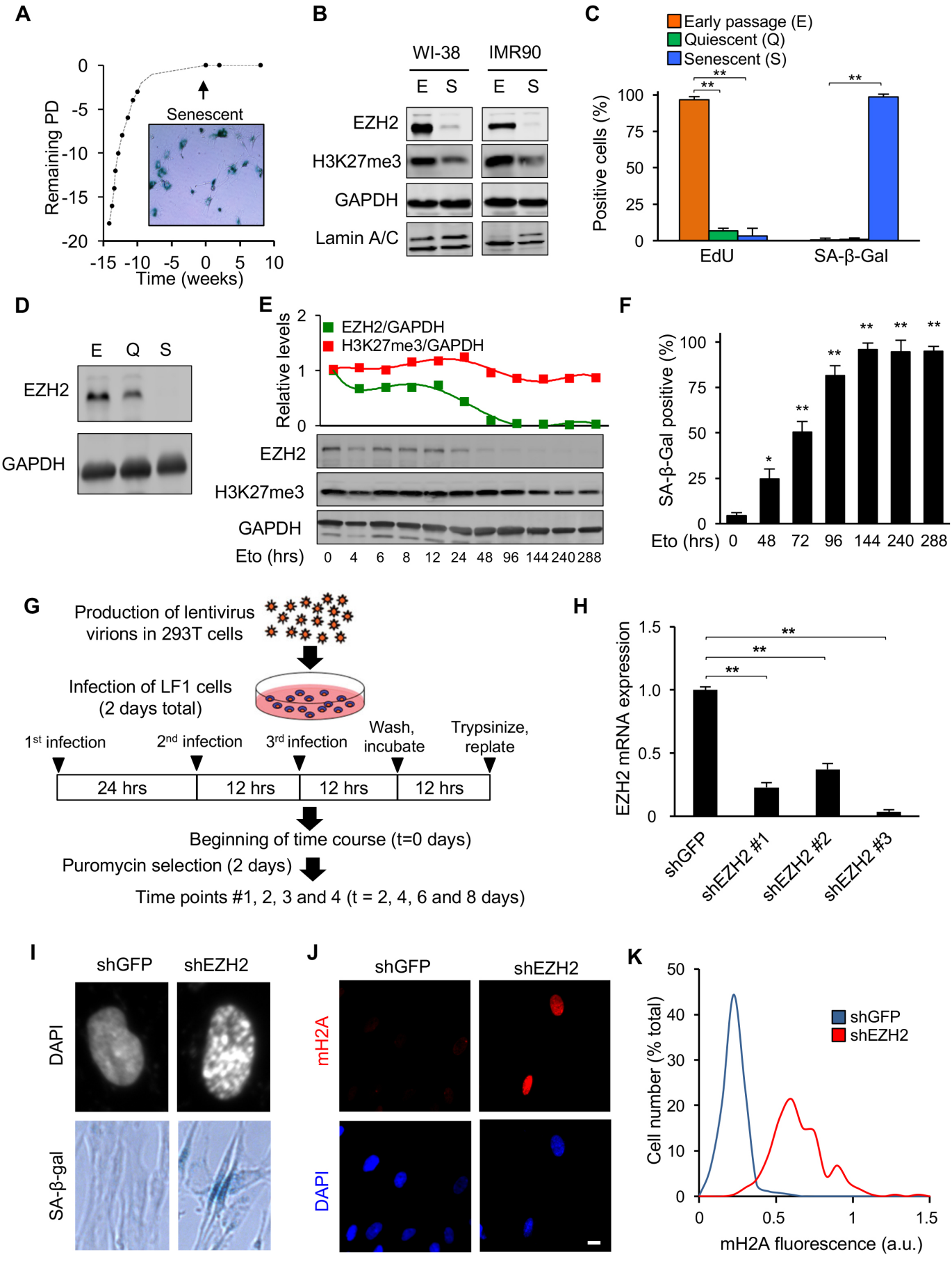
A
Remaining PD
Senescent
Time (weeks)
B
WI-38
IMR90
E S E S
EZH2
H3K27me3
GAPDH
Lamin A/C
C
Early passage (E)
Quiescent (Q)
Senescent (S)
Positive cells (%)
EdU
SA-β-Gal
D
E Q S
EZH2
GAPDH
E
EZH2/GAPDH
H3K27me3/GAPDH
Relative levels
EZH2
H3K27me3
GAPDH
Eto (hrs) 0 4 6 8 12 24 48 96 144 240 288
F
SA-β-Gal positive (%)
Eto (hrs) 0 48 72 96 144 240 288
G
Production of lentivirus virions in 293T cells
Infection of LF1 cells (2 days total)
1st infection
2nd infection
3rd infection
Wash, incubate
Trypsinize, replate
24 hrs
12 hrs
12 hrs
12 hrs
Beginning of time course (t=0 days)
Puromycin selection (2 days)
Time points #1, 2, 3 and 4 (t = 2, 4, 6 and 8 days)
H
EZH2 mRNA expression
shGFP
shEZH2 #1
shEZH2 #2
shEZH2 #3
I
shGFP
shEZH2
DAPI
SA-β-gal
J
shGFP
shEZH2
mH2A
DAPI
K
Cell number (% total)
shGFP
shEZH2
mH2A fluorescence (a.u.)

Figure S1, Related to Figure 1

Expression and Knockdown of EZH2 and Phenotypes of Senescent Cells

(A) Cells were serially propagated under standard culture conditions. Onset of senescence was designated as the zero time point, at which >95% of the cells in the culture were SA-β-Gal positive. The points in the graph correspond to the lanes shown in Figure 1D.

(B) Levels of EZH2 protein and the H3K27me3 mark were examined by immunoblotting in HDF strains WI-38 and IMR90 at early passage (E) and 5 weeks after the onset of senescence (S).

(C) LF1 early passage, replicatively senescent, and serum-starved quiescent cells were assayed for SA-β-Gal activity and EdU incorportation (**$p<0.01$, n=3).

(D) EZH2 protein levels were examined by immunoblotting in samples from panel (C).

(E) Cells were treated with etoposide (Eto, 40 μM) at the zero time point and levels of EZH2 protein and H3K27me3 marks were examined by immunoblotting. EZH2 and H3K27me3 levels were normalized to GAPDH (green and red plots, respectively).

(F) SA-β-Gal positive cells were scored in the etoposide treatment experiment shown in panel (E) (*$p<0.05$, **$p<0.01$, n=3).

(G) Schematic overview and timeline of lentivirus shRNA infection experiments. Cells were infected with lentiviral particles for a total of 2 days. After a wash and 12 hrs further incubation the cultures were replated, and this time point was designated as t=0 for all the time courses presented in this study. Cells were treated with puromycin for 2 days, at which time all sensitive cells had been effectively removed. Cells were harvested at successive time points as indicated in individual experiments.

(H) LF1 cells were infected with lentivirus vectors expressing three different shRNAs against the EZH2 transcript. The effectiveness of knockdowns was examined by RT-qPCR for the EZH2 mRNA 2 days after infection (**$p<0.01$, n=3). shRNA against GFP was used as the control. The shRNAs used are listed in the Extended Experimental Procedures.

(I) EZH2 was knocked down as described in Figure 1E. Representative images of cells displaying SAHF and SA-β-Gal activity are shown. SAHF formation was visualized by DAPI staining. Images were acquired 2 days after infection with EZH2 shRNA.

(J) EZH2 was knocked down as in panel I and mH2A expression was examined using IF microscopy.

(K) mH2A nuclear signals were quantified in the IF images using ImageJ software and plotted as histograms of cell number (% of total) against fluorescent intensity in arbitrary units (a.u.). At least 260 nuclei were observed for each condition.

Error bars represent SD.

A

shEZH2: 4 days after infection

GO Process (Upregulated)	NES	FDR q-val
SYNAPSE_ASSEMBLY	2.223	<0.001
ORGANIC_HYDROXY_COMPOUND_TRANSPORT	2.188	<0.001
TEMPERATURE_HOMEOSTASIS	2.145	<0.001
SYNAPSE_ORGANIZATION	2.141	<0.001
DOPAMINE_METABOLIC_PROCESS	2.107	<0.001

GO Process (Downregulated)	NES	FDR q-val
DNA_STRAND_ELONGATION_INVOLVED_IN_DNA_REPLICATION	-2.564	<0.001
DNA_REPLICATION_INITIATION	-2.541	<0.001
DNA_DEPENDENT_DNA_REPLICATION	-2.517	<0.001
DNA_STRAND_ELONGATION	-2.467	<0.001
DANG_REGULATED_BY_MYC_UP	-2.463	<0.001

B

shEZH2: 8 days after infection

GO Process (Upregulated)	NES	FDR q-val
SASP	2.551	<0.001
CHEMOKINE_MEDIATED_SIGNALING_PATHWAY	2.297	<0.001
LEUKOCYTE_CHEMOTAXIS	2.271	<0.001
CELL_CHEMOTAXIS	2.269	<0.001
MYELOID_LEUKOCYTE_MIGRATION	2.183	<0.001

GO Process (Downregulated)	NES	FDR q-val
SISTER_CHROMATID_SEGREGATION	-3.066	<0.001
CHROMOSOME_SEGREGATION	-3.033	<0.001
NUCLEAR_CHROMOSOME_SEGREGATION	-2.992	<0.001
SISTER_CHROMATID_COHESION	-2.904	<0.001
MITOTIC_SISTER_CHROMATID_SEGREGATION	-2.833	<0.001

C

Top upstream regulators assessed by IPA

Upstream Regulator	Predicted Activation State	Activation z-score	p-value of overlap
ERBB2	Inhibited	-4.95	4.73E-39
TP53	Activated	4.242	9.06E-38
NUPR1	Activated	5.803	7.48E-24
CCND1	Inhibited	-3.408	1.43E-23
MYC	Inhibited	-5.465	3.94E-23
CDKN1A (p21)	Activated	2.544	5.42E-22
TBX2	Inhibited	-6.265	5.90E-22
FOXO3	Activated	3.333	7.78E-22

Genes fold change 1.75 and p<0.05

Figure S2, Related to Figure 1

RNA-seq Analysis of Global Gene Expression Changes Elicited by Knockdown of EZH2

(A-B) EZH2 was knocked down as described in Figure 1E and RNA-seq was performed on RNA harvested on day 4 and 8 after infection. The data were analyzed using GSEA and the top 5 upregulated and downregulated GO process pathways, ranked by normalized enrichment score (NES), are shown for 4 days (A) and 8 days (B) after infection.

(C) Upstream Regulator analysis was performed using IPA and the 8 most activated or inhibited regulators are shown at 8 days after EZH2 knockdown.

See also Tables S4, S5.

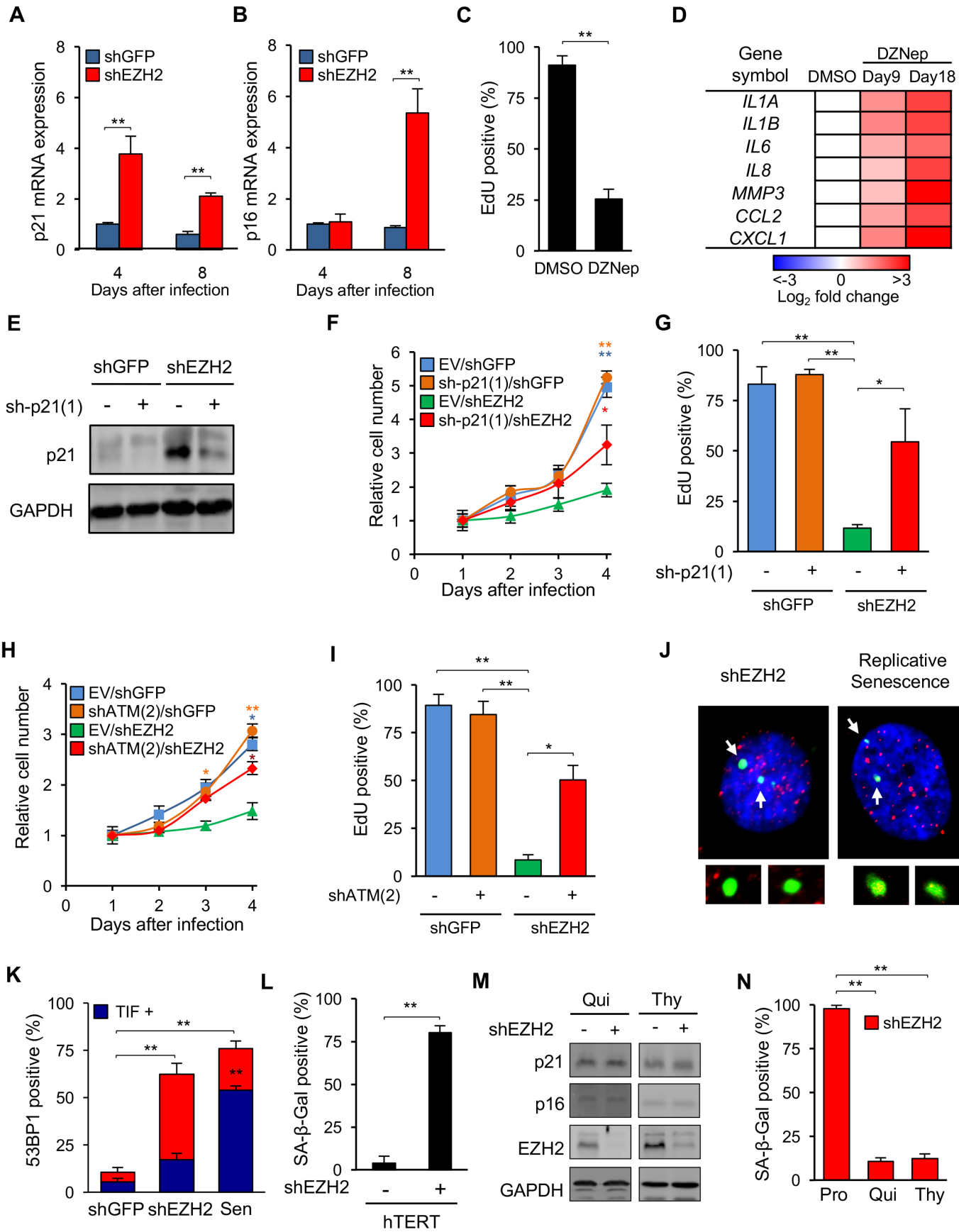
A
p21 mRNA expression
shGFP
shEZH2
Days after infection
B
p16 mRNA expression
C
EdU positive (%)
DMSO DZNep
D
Gene symbol
DZNep
DMSO Day9 Day18
IL1A
IL1B
IL6
IL8
MMP3
CCL2
CXCL1
Log2 fold change
E
shGFP shEZH2
sh-p21(1)
p21
GAPDH
F
Relative cell number
EV/shGFP
sh-p21(1)/shGFP
EV/shEZH2
sh-p21(1)/shEZH2
Days after infection
G
EdU positive (%)
sh-p21(1)
shGFP shEZH2
H
Relative cell number
EV/shGFP
shATM(2)/shGFP
EV/shEZH2
shATM(2)/shEZH2
Days after infection
I
EdU positive (%)
shATM(2)
shGFP shEZH2
J
shEZH2
Replicative Senescence
K
53BP1 positive (%)
TIF +
shGFP shEZH2 Sen
L
SA-β-Gal positive (%)
shEZH2
hTERT
M
Qui Thy
shEZH2
p21
p16
EZH2
GAPDH
N
SA-β-Gal positive (%)
shEZH2
Pro Qui Thy

Figure S3, Related to Figure 2

Cellular Phenotypes Elicited by Knockdown of EZH2

(A) EZH2 was knocked down as in Figure 1E and expression of p21 mRNA was measured by RT-qPCR at 4 and 8 days after infection (**p<0.01, n=3).

(B) Expression of p16 was determined in the experiment shown in (A).

(C) Cells grown continuously in the presence of DZNep (5 μM) for 9 days were assayed for EdU incorporation (**p<0.01, n=3).

(D) Expression of the indicated genes was determined by RT-qPCR in cells treated with DZNep for 9 and 18 days. The data are represented as heat maps relative to vehicle (DMSO) control (n=3).

(E) A double knockdown of EZH2 and p21 was performed as described in Figure 2F, and the levels of p21 protein were determined by immunoblotting. The control for EZH2 knockdown was shGFP, and for p21, the empty vector.

(F-G) A double knockdown of EZH2 and p21 was performed as above and proliferation was assessed by cell number (F) or EdU staining (G) (*p<0.05, **p<0.01, n=3).

(H-I) A double knockdown of EZH2 and ATM was performed and proliferation was assessed by cell numbers (H) or EdU staining (I) (*p<0.05, **p<0.01, n=3).

(J) Replicatively senescent cells or cells made senescent by knockdown of EZH2 were processed for the simultaneous visualization of 53BP1 DNA damage foci (by IF) and telomeres (by FISH). Colocalization of 53BP1 and telomere signals are scored as Telomere dysfunction Induced Foci (TIFs). DNA was counterstained with DAPI (blue). Arrows point to representative enlarged images of 53BP1 DNA damage foci.

(K) The experiment in (J) above was quantified by counting DNA damage foci and TIFs in >150 nuclei per condition. A cell with at least 1 clearly visible 53BP1 focus was scored as a 53BP1-positive cell, and a cell in which ≥50% of 53BP1 foci colocalized with a telomere was scored as a TIF-positive cell. (**p<0.01, n=3). The increase in TIFs in cells infected with shEZH2 was not significant compared to the control (cells infected with shGFP).

(L) EZH2 was knocked down as in (A) in LF1 cells immortalized with human telomerase (hTERT) and SA-β-Gal-positive cells were scored 4 days after infection (**p<0.01, n=3).

(M-N) EZH2 was knocked down as in Figure 2I, and p21, p16 and EZH2 protein levels were determined by immunoblotting (M) or assayed for SA-β-Gal activity (N) 4 days after infection (**p<0.01, n=3).

Error bars represent SD.

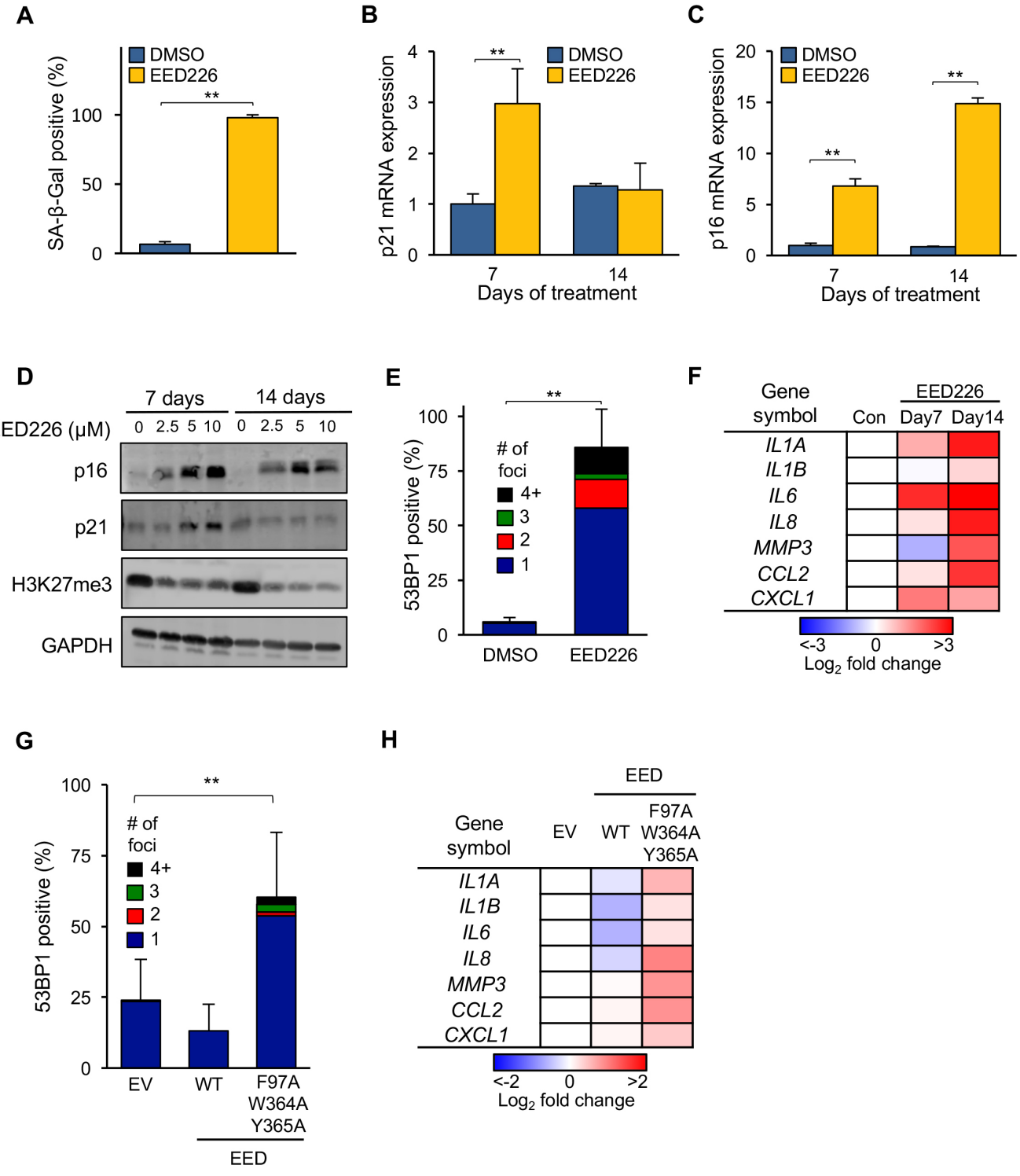
A
SA-β-Gal positive (%)
DMSO
EED226
**
B
p21 mRNA expression
DMSO
EED226
**
7
14
Days of treatment
C
p16 mRNA expression
DMSO
EED226
**
**
7
14
Days of treatment
D
7 days
14 days
EED226 (μM)
0 2.5 5 10 0 2.5 5 10
p16
p21
H3K27me3
GAPDH
E
53BP1 positive (%)
**
# of foci
4+
3
2
1
DMSO
EED226
F
Gene symbol
Con
EED226
Day7
Day14
IL1A
IL1B
IL6
IL8
MMP3
CCL2
CXCL1
<-3
0
>3
Log2 fold change
G
53BP1 positive (%)
**
# of foci
4+
3
2
1
EV
WT
F97A W364A Y365A
EED
H
EED
Gene symbol
EV
WT
F97A W364A Y365A
IL1A
IL1B
IL6
IL8
MMP3
CCL2
CXCL1
<-2
0
>2
Log2 fold change

Figure S4, Related to Figure 2

Inhibition of H3K27me3 Mark Recognition by EED Phenocopies EZH2 Knockdown

(A) Cells were continuously treated with the drug EED226 (10 μM) or vehicle (DMSO) for 7 days and assayed for SA-β-Gal activity (**p<0.01, n=3).

(B-C) Cells were treated with EED226 (10 μM) or DMSO and expression of p21 (B) and p16 (C) mRNA was measured by RT-qPCR at 7 and 14 days (**p<0.01, n=3).

(D) Cells were treated with varying concentrations of EED226 and p16, p21 and H3K27me3 levels were determined by immunoblotting.

(E) Cells were treated as in (A) and 53BP1 foci were visualized by IF after 7 days of drug treatment (**p<0.01, n=3).

(F) Expression of the indicated genes was determined by RT-qPCR in cells treated with EED226 (10 μM) or DMSO control at 7 and 14 days. The data are represented as heat maps relative to the DMSO control (n=3).

(G) Cells were infected with lentivirus vectors to ectopically express WT *EED* cDNA or *EED*(F97A/W364A/Y365A) mutated cDNA and p16, p21 and H3K27me3 levels were scored for 53BP1 foci as in (E) (**p<0.01, n=3).

(H) Cells ectopically expressing WT *EED* or *EED*(F97A/W364A/Y365A) cDNAs (experiment in (G) above) were assessed for the expression of the indicated genes as in (F).

Error bars represent SD.

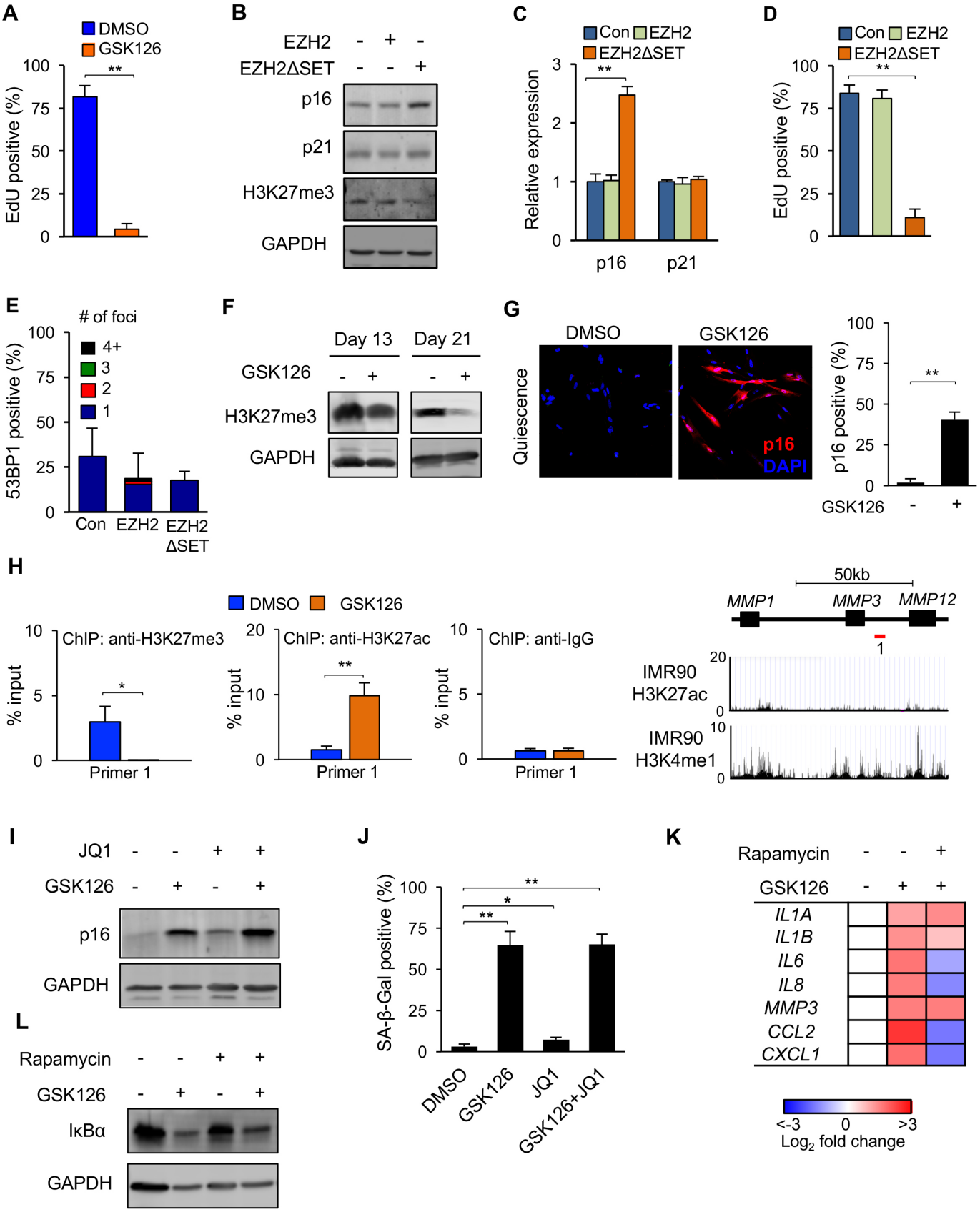
A
DMSO
GSK126
EdU positive (%)
100
75
50
25
0
**
B
EZH2 - + -
EZH2ΔSET - - +
p16
p21
H3K27me3
GAPDH
C
Con EZH2
EZH2ΔSET
Relative expression
3
2
1
0
**
p16
p21
D
Con EZH2
EZH2ΔSET
EdU positive (%)
100
75
50
25
0
**
E
# of foci
4+
3
2
1
53BP1 positive (%)
100
75
50
25
0
Con
EZH2
EZH2 ΔSET
F
Day 13
Day 21
GSK126 - + - +
H3K27me3
GAPDH
G
DMSO
GSK126
Quiescence
p16
DAPI
p16 positive (%)
100
75
50
25
0
**
GSK126 - +
H
DMSO
GSK126
ChIP: anti-H3K27me3
% input
10
5
0
*
Primer 1
ChIP: anti-H3K27ac
% input
20
10
0
**
Primer 1
ChIP: anti-IgG
% input
10
5
0
Primer 1
50kb
MMP1
MMP3
MMP12
1
IMR90
H3K27ac
20
0
IMR90
H3K4me1
10
0
I
JQ1 - - + +
GSK126 - + - +
p16
GAPDH
J
SA-β-Gal positive (%)
100
75
50
25
0
**
*
**
DMSO
GSK126
JQ1
GSK126+JQ1
K
Rapamycin - - +
GSK126 - + +
IL1A
IL1B
IL6
IL8
MMP3
CCL2
CXCL1
<-3
0
>3
Log2 fold change
L
Rapamycin - - + +
GSK126 - + - +
IκBα
GAPDH

Figure S5, Related to Figure 3

Inhibition of EZH2 Activity Induces Senescence by Depleting H3K27me3 Marks and Activating p16 and SASP Genes

(A) Cells were continuously treated with the drug GSK126 (5 μM) or vehicle (DMSO) for 20 days and then assayed for EdU incorporation (** $p<0.01$, n=3).

(B) Cells were infected with lentivirus vectors expressing *EZH2* or *EZH2ΔSET* cDNAs, or empty vector as control (as in Figure 3G), and p16, p21 and H3K27me3 levels were determined by immunoblotting 9 days after infection.

(C-D) In the experiment shown in (B) above, expression of p16 and p21 mRNAs was determined by RT-qPCR (C) and proliferation was assessed by EdU incorporation (D) (** $p<0.01$, n=3).

(E) In the experiment shown in (B) above, 53BP1 foci were visualized by IF (n=3).

(F) Cells were made quiescent by incubation in medium supplemented with 0.25% FBS and then treated with GSK126 (5 μM) for the indicated times. Levels of the H3K27me3 mark were determined by immunoblotting.

(G) Cells were treated with GSK as in (F) above for 21 days and immunostained with antibodies to p16. Nuclei were counterstained with DAPI. The frequency of p16-expressing cells is shown in the right panel (% of total cells, random fields, >200 cells per condition, **$p<0.01$).

(H) Cells were treated with GSK126 (5 μM) or DMSO for 10 days and H3K27me3 and H3K27ac enrichment at the enhancer between the *MMP3* and *MMP12* loci was determined by ChIP-qPCR. Normal rabbit IgG was used as the IP control (** $p<0.01$, n=3). Location of the primer pair is indicated in the schematic on right. The IMR90 H3K27ac and H3K4me1 tracks were obtained from ENCODE (GEO ID: GSM469966 and GSM521895).

(I) Cells were treated with GSK126 (5 μM), JQ1 (100 nM) or both, and levels of the p16 protein were determined by immunoblotting after 10 days.

(J) Cells were treated as in (I) and the frequency of SA-β-Gal positive cells was determined (* $p<0.05$, ** $p<0.01$, n=3).

(K) Cells were treated with GSK126 for 10 days, followed by 4 days of combined treatment with GSK126 and rapamycin (12.5 nM). Expression of the indicated SASP genes was determined by RT-qPCR (n=3). The data are expressed as heat maps relative to control (vehicle-treated) cells.

(L) Cells were treated as in (K) and IκBα protein levels were determined by immunoblotting. Error bars represent SD.

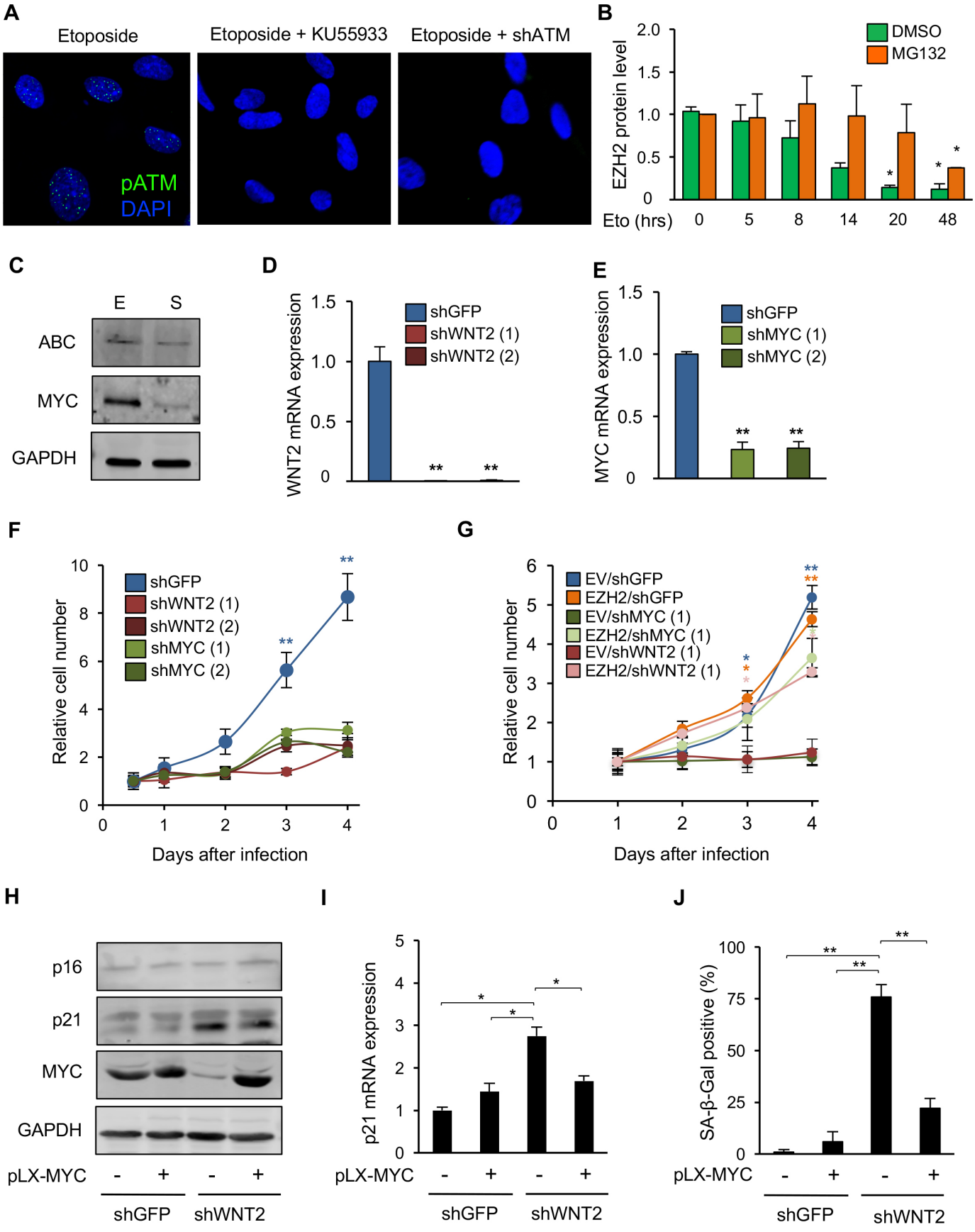
A
Etoposide
Etoposide + KU55933
Etoposide + shATM
pATM
DAPI
B
DMSO
MG132
EZH2 protein level
Eto (hrs)
0
5
8
14
20
48
C
E
S
ABC
MYC
GAPDH
D
shGFP
shWNT2 (1)
shWNT2 (2)
WNT2 mRNA expression
E
shGFP
shMYC (1)
shMYC (2)
MYC mRNA expression
F
shGFP
shWNT2 (1)
shWNT2 (2)
shMYC (1)
shMYC (2)
Relative cell number
Days after infection
G
EV/shGFP
EZH2/shGFP
EV/shMYC (1)
EZH2/shMYC (1)
EV/shWNT2 (1)
EZH2/shWNT2 (1)
Relative cell number
Days after infection
H
p16
p21
MYC
GAPDH
pLX-MYC
shGFP
shWNT2
I
p21 mRNA expression
pLX-MYC
shGFP
shWNT2
J
SA-β-Gal positive (%)
pLX-MYC
shGFP
shWNT2

Figure S6, Related to Figure 5 and Figure 6

Regulation of EZH2 Expression by ATM and WNT-MYC Signaling

(A) Cells were treated with etoposide (40 μM, left panel), etoposide plus the ATM inhibitor KU-55933 (10 μM, middle panel), or with etoposide and infected with shRNA against ATM (right panel), and immunostained with antibodies to phospho-ATM (S1981). Nuclei were counterstained with DAPI.

(B) Cells were treated with etoposide (40 μM) with or without the proteasome inhibitor MG132 (10 μM) and levels of EZH2 protein were determined by immunoblotting. GAPDH was used as the loading control (* $p<0.05$, calculated relative to t=0 time point, n=2).

(C) Levels of active β-catenin (ABC) and MYC protein were examined by immunoblotting in early passage cells and 2 weeks after the onset of replicative senescence.

(D-E) Cells were infected with lentivirus vectors expressing two different shRNAs against the WNT2 or MYC transcripts. The effectiveness of knockdowns was examined by RT-qPCR for the WNT2 (D) or MYC (E) mRNAs 2 days after infection (** $p<0.01$, n=3). shRNA against GFP was used as the control. The shRNAs used are listed in the Extended Experimental Procedures.

(F) WNT2 or MYC were knocked down as in (D) and (E) above and proliferation was assessed by counting cell numbers (** $p<0.01$, n=3).

(G) Ectopic expression of *EZH2* cDNA was combined with a shRNA knockdown of WNT2 or MYC and proliferation was assessed by counting cell numbers (** $p<0.01$, n=3).

(H) Ectopic expression of *MYC* cDNA was combined with a shRNA knockdown of WNT2. Controls were empty pLX lentivirus vector for *MYC* (–) and shGFP for WNT2. Levels of p16, p21, and MYC proteins were determined by immunoblotting. Note that while endogenous MYC expression is effectively downregulated by shWNT2 (lane 3), ectopic expression is maintained by the pLX-MYC vector (lane 4).

(I) p21 mRNA expression was determined by RT-qPCR in the experiment shown in (H) (* $p<0.05$, n=3).

(J) The presence of SA-β-Gal positive cells was scored in the experiment shown in (H) (** $p<0.01$, n=3).

Error bars represent SD.

Table S1, Related to Experimental Procedures

List of primer sequences for RT-qPCR

Gene	Orientation	Sequences (5' to 3')
EZH2	Sense	GCAACACCCAACACTTATAAGC
	Antisense	CTCCCTCCAAATGCTGGTA
WNT2	Sense	TGGCAGGAAGGCTGTAAAGC
	Antisense	ATGGCCAGCCAGCATGTC
MYC	Sense	GGATTCTCTGCTCTCCTCGAC
	Antisense	TTGTTCCTCCTCAGAGTCGC
IL1A	Sense	GAGAGCATGGTGGTAGTAGCAA
	Antisense	AGGCTTGATGATTTCTTCCTCTGA
IL1B	Sense	CGCCAGTGAAATGATGGCTTAT
	Antisense	CTGGAAGGAGCACTTCATCTGT
MMP3	Sense	CCCACCTTACATACAGGATTGTGA
	Antisense	CCCAGACTTTCAGAGCTTTCTCA
IL6	Sense	CACTGGCAGAAAACAACCTGAA
	Antisense	ACCAGGCAAGTCTCCTCATTGA
CXCL8 (IL8)	Sense	GTTTTTGAAGAGGGCTGAGAATTC
	Antisense	CCCTACAACAGACCCACACAATAC
CCL2	Sense	AAGACCATTGTGGCCAAGGA
	Antisense	TTCGGAGTTTGGGTTTGCT
CXCL1	Sense	CAATCCTGCATCCCCCATAG
	Antisense	CAGCCACCAGTGAGCTTCCT
CDKN2A (p16-INK4A)	Sense	CGGAAGGTCCCTCAGACATC
	Antisense	CCCTGTAGGACCTTCGGTGA
CDKN1A (p21-CIP1)	Sense	GAGACTCTCAGGGTCGAAAACG
	Antisense	TTCCTGTGGGCGGATTAGG
GAPDH	Sense	GGAGTCAACGGATTTGGTCGT
	Antisense	GTTGAGGTCAATGAAGGGGTCA

Table S2, Related to Experimental Procedures

List of primer sequences for ChIP-qPCR

Gene/location	Orientation	Sequences (5' to 3')	Notes
ARF Exon 1β	Sense	GTGGGTCCCAGTCTGCAGTTA	Fig. 2A, #1
	Antisense	CCTTTGGCACCAGAGGTGAG	
15 kb downstream of *ARF* promoter	Sense	GCACTTGCCCTTCCAGGTATA	Fig. 2A, #2
	Antisense	TGATAGTTCAAGGCCCTATGCC	
200 bp upstream *p16-INK4A* TSS	Sense	ACCCCGATTCAATTTGGCAG	Fig. 2A, #3
	Antisense	AAAAAGAAATCCGCCCCCG	
p16-INK4A, exon 1α	Sense	AGAGGGTCTGCAGCGG	Fig. 2A, #4
	Antisense	TCGAAGCGCTACCTGATTCC	
200 bp downstream of *p16-INK4A* exon 1α	Sense	GCCAAGGAAGAGGAATGAGGAG	Fig. 2A, #5
	Antisense	CCTTCAGATCTTCTCAGCATTCG	
678 bp upstream of *IL1A*	Sense	GCTGACTCAAACGCCAATGAAA	Fig. 3J, #1
	Antisense	CGTTTTGACGACGCACTTGTAG	
11490 bp upstream of *IL1A*	Sense	CAGGACCCATGCTAGACACATT	Fig. 3J, #2
	Antisense	CGAAGTAAAGCAGAAAGAGCGT	
20187 bp upstream of *IL1A*	Sense	GTGCCTGTTGACAGTAAGGCAT	Fig. 3J, #3
	Antisense	TGGCATCCAAAACAGGTGTCAA	
28917 bp upstream of *IL1A*	Sense	TACTAGGGCCCAGGAGAGTTAC	Fig. 3J, #4
	Antisense	CCTCACGCCATAGCTATTCACA	
5567 bp downstream of *IL1B*	Sense	CCACATGCTGCATTTCATGGTT	Fig. 3J, #5
	Antisense	GGAAGTCCAGAAGCACTCCTTT	
3756 bp upstream of *IL1B*	Sense	CCAGCTAAGAGGAGCCCTAATG	Fig. 3J, #6
	Antisense	ATGAGTCACTTCCACCCTCCTA	
32953 bp upstream of *IL1B*	Sense	AGTGAGCAAGAGTTCTGGATTGT	Fig. 3J, #7
	Antisense	ACCAGTCACTGCTTTGTTTCTG	
45347 bp upstream of *IL1B*	Sense	AATCATAAGTCAGGAGGGCCAC	Fig. 3J, #8
	Antisense	TGTCTGGCCATTTAAGTCACGA	
6898 bp upstream of *MMP3*	Sense	TATCTGGTGGCAGTGATTGAGA	Fig. S5H, #1
	Antisense	TATCTGCAGTCCTTCGGGTTG	
EZH2, 1034 bp upstream of TSS	Sense	ACATTGCTGCCATTTCAGAC	Fig. 6C, #1
	Antisense	AGTGAACAGTGCTCATCTTGA	
EZH2, 156 bp upstream of TSS	Sense	TTCGCTGTAAGGGACGC	Fig. 6C, #2
	Antisense	TGTGTTCAGCGAAAGAACAA	
EZH2 TSS	Sense	CCAATCGCCATCGCTTTTAT	Fig. 6C, #3
	Antisense	GGGCCCTGTGATTGGAC	

Table S3, Related to Figure 3

Assay of Conditioned Media for Cytokine Production

CONDITION[1]	GENE SYMBOL	CONCENTRATION (pg/ml)
CTR #1	IL1A	117.875
CTR #1	IL1B	140.9496
CTR #1	IL2	15.0576
CTR #1	IL4	39.3584
CTR #1	IL5	24.906
CTR #1	IL6	22.4068
CTR #1	IL8	3.4572
CTR #1	IL10	96.278
CTR #1	IL12	8.7362
CTR #1	IL13	6.1605
CTR #1	CSF2	27.6012
CTR #1	CXCL1	77.3528
CTR #1	IFNG	153.7699
CTR #1	CCL2	90.0836
CTR #1	CCL3	314.4603
CTR #1	CCL4	12.4705
CTR #1	MMP9	131.8152
CTR #1	CCL5	27.0336
CTR #1	TNF	16.115
CTR #1	VEGF	918.7487
CTR #2	IL1A	115
CTR #2	IL1B	136.6784
CTR #2	IL2	14.1165
CTR #2	IL4	39.3584
CTR #2	IL5	24.906
CTR #2	IL6	20.6832
CTR #2	IL8	3.0444
CTR #2	IL10	89.999
CTR #2	IL12	8.0465
CTR #2	IL13	5.8867
CTR #2	CSF2	27.6012
CTR #2	CXCL1	66.3024
CTR #2	IFNG	147.2265
CTR #2	CCL2	74.1396
CTR #2	CCL3	304.9312
CTR #2	CCL4	12.1142
CTR #2	MMP9	127.8208
CTR #2	CCL5	27.0336
CTR #2	TNF	16.4373
CTR #2	VEGF	680.2715
GSK126+JQ1 #1	IL1A	117.875
GSK126+JQ1 #1	IL1B	136.6784
GSK126+JQ1 #1	IL2	15.9987
GSK126+JQ1 #1	IL4	40.516
GSK126+JQ1 #1	IL5	25.499
GSK126+JQ1 #1	IL6	96.5216
GSK126+JQ1 #1	IL8	7.0692
GSK126+JQ1 #1	IL10	96.278
GSK126+JQ1 #1	IL12	8.9661
GSK126+JQ1 #1	IL13	6.4343
GSK126+JQ1 #1	CSF2	30.1104
GSK126+JQ1 #1	CXCL1	103.5975
GSK126+JQ1 #1	IFNG	153.7699
GSK126+JQ1 #1	CCL2	217.6356
GSK126+JQ1 #1	CCL3	323.9894

GSK126+JQ1 #1	CCL4	12.8268
GSK126+JQ1 #1	MMP9	135.8096
GSK126+JQ1 #1	CCL5	27.0336
GSK126+JQ1 #1	TNF	17.7265
GSK126+JQ1 #1	VEGF	524.3441
GSK126+JQ1 #2	IL1A	115
GSK126+JQ1 #2	IL1B	145.2208
GSK126+JQ1 #2	IL2	15.3713
GSK126+JQ1 #2	IL4	50.9344
GSK126+JQ1 #2	IL5	25.499
GSK126+JQ1 #2	IL6	109.8795
GSK126+JQ1 #2	IL8	5.16
GSK126+JQ1 #2	IL10	104.65
GSK126+JQ1 #2	IL12	8.7362
GSK126+JQ1 #2	IL13	7.2557
GSK126+JQ1 #2	CSF2	29.4831
GSK126+JQ1 #2	CXCL1	95.3097
GSK126+JQ1 #2	IFNG	150.4982
GSK126+JQ1 #2	CCL2	235.174
GSK126+JQ1 #2	CCL3	314.4603
GSK126+JQ1 #2	CCL4	12.8268
GSK126+JQ1 #2	MMP9	131.8152
GSK126+JQ1 #2	CCL5	27.8784
GSK126+JQ1 #2	TNF	17.4042
GSK126+JQ1 #2	VEGF	454.0239
GSK126 #1	IL1A	132.25
GSK126 #1	IL1B	140.9496
GSK126 #1	IL2	17.8809
GSK126 #1	IL4	42.8312
GSK126 #1	IL5	30.243
GSK126 #1	IL6	10455.3576
GSK126 #1	IL8	278.2788
GSK126 #1	IL10	119.301
GSK126 #1	IL12	9.6558
GSK126 #1	IL13	8.8985
GSK126 #1	CSF2	43.911
GSK126 #1	CXCL1	1164.4359
GSK126 #1	IFNG	173.4001
GSK126 #1	CCL2	2134.1044
GSK126 #1	CCL3	343.0476
GSK126 #1	CCL4	14.6083
GSK126 #1	MMP9	135.8096
GSK126 #1	CCL5	29.568
GSK126 #1	TNF	19.0157
GSK126 #1	VEGF	3321.8651
GSK126 #2	IL1A	115
GSK126 #2	IL1B	166.5768
GSK126 #2	IL2	16.9398
GSK126 #2	IL4	40.516
GSK126 #2	IL5	23.72
GSK126 #2	IL6	5046.2699
GSK126 #2	IL8	224.1504
GSK126 #2	IL10	100.464
GSK126 #2	IL12	8.7362
GSK126 #2	IL13	8.4878
GSK126 #2	CSF2	37.0107
GSK126 #2	CXCL1	868.8377
GSK126 #2	IFNG	170.1284
GSK126 #2	CCL2	1387.128
GSK126 #2	CCL3	323.9894
GSK126 #2	CCL4	13.1831

GSK126 #2	MMP9	135.8096
GSK126 #2	CCL5	28.7232
GSK126 #2	TNF	18.3711
GSK126 #2	VEGF	1872.6575
shEZH2 #1	IL1A	140.875
shEZH2 #1	IL1B	149.492
shEZH2 #1	IL2	20.3905
shEZH2 #1	IL4	45.1464
shEZH2 #1	IL5	31.429
shEZH2 #1	IL6	24071.7976
shEZH2 #1	IL8	758.8296
shEZH2 #1	IL10	198.835
shEZH2 #1	IL12	10.5754
shEZH2 #1	IL13	12.4579
shEZH2 #1	CSF2	148.6701
shEZH2 #1	CXCL1	16943.0258
shEZH2 #1	IFNG	199.5737
shEZH2 #1	CCL2	5057.4368
shEZH2 #1	CCL3	371.6349
shEZH2 #1	CCL4	17.1024
shEZH2 #1	MMP9	159.776
shEZH2 #1	CCL5	32.9472
shEZH2 #1	TNF	22.561
shEZH2 #1	VEGF	4073.9855
shEZH2 #2	IL1A	126.5
shEZH2 #2	IL1B	158.0344
shEZH2 #2	IL2	19.4494
shEZH2 #2	IL4	48.6192
shEZH2 #2	IL5	27.871
shEZH2 #2	IL6	12237.9909
shEZH2 #2	IL8	617.7552
shEZH2 #2	IL10	182.091
shEZH2 #2	IL12	10.5754
shEZH2 #2	IL13	10.8151
shEZH2 #2	CSF2	124.2054
shEZH2 #2	CXCL1	13926.2666
shEZH2 #2	IFNG	179.9435
shEZH2 #2	CCL2	3494.1276
shEZH2 #2	CCL3	343.0476
shEZH2 #2	CCL4	15.3209
shEZH2 #2	MMP9	143.7984
shEZH2 #2	CCL5	30.4128
shEZH2 #2	TNF	19.9826
shEZH2 #2	VEGF	2432.1617

[1] CTR, Control.

Table S4, Related to Figures 1 and S2.

Alignment Rates of RNA-seq Data

Sample	Number of reads	Reads after trimming	% of reads remaining	HISAT2 alignment %	% aligned concordantly exactly 1 time	# aligned concordantly exactly 1 time	FeatureCount gene count
shGFP_1	39,544,533	39,493,427	99.87	96.17	87.73	34,647,571	32,177,852
shGFP_2	33,331,456	33,293,441	99.89	96.1	88.73	29,541,575	27,440,073
shGFP_3	31,621,901	31,581,385	99.87	96.01	88.33	27,894,550	25,876,556
shEZH2_4hr_1	30,174,636	30,145,492	99.90	95.72	88.56	26,696,692	24,665,826
shEZH2_4hr_2	27,559,330	27,532,883	99.90	95.33	87.76	24,163,287	22,260,670
shEZH2_4hr_3	32,452,763	32,420,262	99.90	96.2	88.15	28,578,966	26,016,533
shEZH2_8hr_1	34,542,173	34,496,893	99.87	94.39	86.3	29,771,809	27,425,389
shEZH2_8hr_2	34,805,705	34,770,894	99.90	94.27	86.55	30,094,531	27,588,381
shEZH2_8hr_3	33,358,345	33,326,622	99.90	94.86	88.64	29,540,951	27,126,907

SUPPLEMENTAL REFERENCES

Debacq-Chainiaux, F., Erusalimsky, J.D., Campisi, J., and Toussaint, O. (2009). Protocols to detect senescence-associated beta-galactosidase (SA-betagal) activity, a biomarker of senescent cells in culture and in vivo. Nat. Protoc. *4*, 1798-1806.

Herbig, U., Jobling, W.A., Chen, B.P., Chen, D.J., and Sedivy, J.M. (2004). Telomere shortening triggers senescence of human cells through a pathway involving ATM, p53, and p21(CIP1), but not p16(INK4a). Mol. Cell *14*, 501-513.

Kreiling, J.A., Tamamori-Adachi, M., Sexton, A.N., Jeyapalan, J.C., Munoz-Najar, U., Peterson, A.L., Manivannan, J., Rogers, E.S., Pchelintsev, N.A., Adams, P.D., et al. (2011). Age-associated increase in heterochromatic marks in murine and primate tissues. Aging Cell *10*, 292-304.

Liao, Y., Smyth, G.K., and Shi, W. (2014). featureCounts: an efficient general purpose program for assigning sequence reads to genomic features. Bioinformatics *30*, 923-930.

Love, M.I., Huber, W., and Anders, S. (2014). Moderated estimation of fold change and dispersion for RNA-seq data with DESeq2. Genome Biology *15*, 550.

Moffat, J., Grueneberg, D.A., Yang, X., Kim, S.Y., Kloepfer, A.M., Hinkle, G., Piqani, B., Eisenhaure, T.M., Luo, B., Grenier, J.K., et al. (2006). A lentiviral RNAi library for human and mouse genes applied to an arrayed viral high-content screen. Cell 124, 1283-1298.

Ortega-Atienza, S., Wong, V.C., DeLoughery, Z., Luczak, M.W., and Zhitkovich, A. (2015). ATM and KAT5 safeguard replicating chromatin against formaldehyde damage. Nucleic Acids Res. *44*, 198-209.

Stewart, S.A., Dykxhoorn, D.M., Palliser, D., Mizuno, H., Yu, E.Y., An, D.S., Sabatini, D.M., Chen, I.S., Hahn, W.C., Sharp, P.A., et al. (2003). Lentivirus-delivered stable gene silencing by RNAi in primary cells. RNA *9*, 493-501.

Subramanian, A., Tamayo, P., Mootha, V.K., Mukherjee, S., Ebert, B.L., Gillette, M.A., Paulovich, A., Pomeroy, S.L., Golub, T.R., Lander, E.S., et al. (2005). Gene set enrichment analysis: a knowledge-based approach for interpreting genome-wide expression profiles. Proc. Natl. Acad. Sci. USA *102*, 15545-15550.